



# Linking large-scale climate oscillations to local wave climate and storm surge: insights from a weather typing approach

Zehua Zhong<sup>1</sup>, Hachem Kassem<sup>1</sup>, Ivan D. Haigh<sup>1</sup>, Dafni E. Sifnioti<sup>2</sup>, Ye Liu<sup>3</sup>, and Paula Camus<sup>4,5,1</sup>

Correspondence: Zehua Zhong (Zehua.Zhong@soton.ac.uk)

Abstract. Understanding temporal variations in nearshore sea states is crucial, as they affect shoreline evolution and coastal hazard potential. Local sea state conditions are influenced by daily synoptic weather patterns and by large-scale climate oscillations. Although the underlying mechanisms remain not fully understood, numerous studies have established the links between interannual climate patterns and local sea state variability. While most existing research has relied on correlation analyses or other statistical methods, this study explores the possibility of using a weather typing approach to relate climate oscillation patterns to local wave climate and storm surge. The analysis was conducted at Hartlepool, UK, where 36 weather types were previously developed to assess the exposure to coastal hazards for a local nuclear power station. Six climate indices were examined, and we found that the North Atlantic Oscillation (NAO) and the Scandinavian pattern (SCAND) have significant correlations with local wave and storm surge variables. The weather type analysis reveals that, in response to the phases of NAO or SCAND, storm surge distributions exhibit changes in the mean and standard deviation, peak wave period distributions shift between bimodal and near-unimodal shapes, and wind waves and swell show different dominant directions. These response patterns are attributable to the impacts of atmospheric pressure, wind forcing, and extratropical storm frequency, which are modulated by large-scale climate dynamics associated with NAO and SCAND. This research demonstrates the potential of weather types to offer new perspectives into the impact of climate oscillations on local sea states.

#### 15 1 Introduction

Large-scale climate oscillation patterns are periodic variations in the Earth's climate system that occur over timescales ranging from years to decades. One notable example is the North Atlantic Oscillation (NAO), the leading mode of climate variability in the Euro-Atlantic region, which involves the redistribution of atmospheric mass between the Arctic and the subtropical Atlantic (Hurrell et al., 2003). Alongside NAO, the East Atlantic pattern (EA), the Scandinavian pattern (SCAND), and the Western Europe Pressure Anomaly (WEPA) are also identified as significant modes of climate variability in this region. It has long been recognized that shifts between phases of these climate modes can bring profound changes to surface temperature,

<sup>&</sup>lt;sup>1</sup>School of Ocean and Earth Science, University of Southampton, European Way, Southampton, SO14 3ZH, United Kingdom

<sup>&</sup>lt;sup>2</sup>EDF Research & Development UK Centre, 11 Bressenden Place, London, SW1E 5BY, United Kingdom

<sup>&</sup>lt;sup>3</sup>HR Wallingford, Howbery Park, Wallingford, OX10 8BA, United Kingdom

<sup>&</sup>lt;sup>4</sup>Departamento de Matemática Aplicada y Ciencias de la Computación (MACC), Universidad de Cantabria, 39005 Santander, Spain

<sup>&</sup>lt;sup>5</sup>Geomatics and Ocean Engineering Group, Departamento de Ciencias y Técnicas del Agua y del Medio Ambiente, E.T.S.I.C.C.P., Universidad de Cantabria, 39005 Santander, Spain



40



precipitation, wind patterns, and other meteorological properties (Lamb and Peppler, 1987; Hurrell, 1995; Hurrell et al., 2003). More recently, studies have increasingly focused on their broader impacts beyond the climate system. Significant correlations have been identified with oceanographic variables including wave climate (e.g., Martínez-Asensio et al., 2016; Odériz et al., 2020; Scott et al., 2021) and water level/storm surge (e.g., Wakelin et al., 2003; Woodworth et al., 2007; Chafik et al., 2017). Moreover, the influence on sea state conditions has been further linked to shoreline variability (e.g., Wiggins et al., 2020; Masselink et al., 2023), flood exposure (e.g., Muis et al., 2018; Arcodia et al., 2024), and coastal vulnerability (e.g., Barnard et al., 2015).

Research into the impacts of climate oscillation patterns has significant implications. A deeper understanding of how coastal environments respond to climate variability will enable the use of climate projections to identify areas vulnerable to coastal flooding and erosion driven by climate change, supporting coastal management and adaptation strategies (Barnard et al., 2015; Wiggins et al., 2020). By establishing more robust relationships between large-scale climate oscillations and local-scale environmental drivers, there is also the potential to utilize climate indices for improved reproduction of sea state conditions and better forecasting of coastal change. Hilton et al. (2020) demonstrated that a shoreline prediction model achieved increased accuracy when its synthetic wave generation algorithm was informed by a prior knowledge of the NAO and WEPA indices. In other studies, climate indices were incorporated as predictors to represent interannual or intra-seasonal climate variabilities in stochastic emulators of water levels (Anderson et al., 2019) and wave climate (Cagigal et al., 2020). In addition, understanding these relationships allows for the investigation of historical coastal evolution using reconstructions of climate indices over centennial timescales, offering valuable insights into long-term coastal variability (Wiggins et al., 2020).

Numerous studies have established links between climate oscillations and sea state variability by analysing the temporal correlation between climate indices and specific sea state parameters, such as significant wave height and extreme sea level (e.g., Semedo et al., 2015; Morales-Márquez et al., 2020; Scott et al., 2021; Freitas et al., 2022). These relationships are usually displayed in 2D maps to reflect the spatial patterns and to identify places with robust links, often supplemented by regression coefficients as a measure of the sensitivity of sea state variability to climate indices (e.g., Wakelin et al., 2003; Woodworth et al., 2007; Hochet et al., 2021). Regression analysis has also been employed to evaluate combinations of indices in situations where a singular index fails to fully explain observed variance (e.g., Frederikse and Gerkema, 2018; Scott et al., 2021), thereby providing insights into the relative contribution from each index (Frederikse and Gerkema, 2018). More complicated statistical techniques, including Empirical Orthogonal Function, Canonical Correlation Analysis, and Redundancy Analysis, have also been applied to associate patterns of variations between atmospheric circulation and sea state parameters (e.g., Wang and Swail, 2001; Woolf et al., 2002; Chafik et al., 2017; Hochet et al., 2021).

Meanwhile, climate variability is also widely investigated through weather regimes (e.g., Hurrell et al., 2003; Cassou et al., 2004; Pohl and Fauchereau, 2012), which are recurrent (occur repeatedly), persistent (last for multiple days, e.g., 10 days), and quasi-stationary (large-scale motion is stationary in the statistical sense) atmospheric circulation patterns (Michelangeli et al., 1995). The underlying idea is that the continuously evolving weather system can be represented by a finite set of weather regimes, often obtained by clustering techniques. This concept enables the analysis of atmospheric circulation dynamics across different timescales by examining the temporal distribution of these regimes.

https://doi.org/10.5194/egusphere-2025-5400 Preprint. Discussion started: 19 November 2025

© Author(s) 2025. CC BY 4.0 License.





Beyond understanding climate dynamics, the concept of weather regimes has also influenced downscaling studies, where a similar but distinct approach, often referred to as weather typing, is used to link localized atmospheric or oceanographic information with synoptic-scale weather conditions (Wilby and Wigley, 1997). A key distinction lies in the number of patterns used: downscaling typically requires a larger set (around 30–100) to capture subtle variations in atmospheric circulation and improve the estimation of local variables, whereas studies of low-frequency climate variability focus on broader-scale features and can be effectively represented by fewer patterns (usually no more than 8 (Michelangeli et al., 1995)). Consequently, weather types (WTs) tend to have shorter durations and more frequent transitions, which may not fully align with the definition of a weather regime. Nevertheless, previous work showed that weather types could be associated with certain climate oscillation patterns (e.g., Camus et al., 2014; Neal et al., 2016), highlighting their potential to connect the variability of large-scale climate circulation and local sea states.

In this research, we explore the possibility of relating climate oscillation patterns with local wave climate and storm surge through weather types, an approach not commonly adopted in previous studies. The method's ability to characterize detailed, local multivariate sea state conditions while tracing back the synoptic conditions responsible for them can potentially offer new insights into the role climate oscillation plays in affecting regional hydrodynamics. This work has three objectives: (1) identify the climate oscillation patterns contributing to the sea state variability at the selected location; (2) characterize the responses of storm surge and wave under different phases of the identified climate patterns; and (3) identify the atmospheric processes linking climate oscillations to the corresponding sea state responses.

#### 2 Data and method

This study is part of a broader project assessing coastal hazard exposure at UK nuclear power stations using a hybrid statistical-dynamical downscaling approach. We applied the weather typing method at the Hartlepool nuclear power station, which is located on the north-east coast of England (Fig. 1). A set of 36 WTs was developed to characterize the regional synoptic circulation patterns, which were then linked to the wave and storm surge conditions at an offshore location near the nuclear station. This research expands upon our previous work (Zhong et al., 2025) by incorporating large-scale climate oscillation patterns into the weather type analysis.

## 2.1 Weather typing

The weather typing method was originally developed in Camus et al. (2014) and later applied and validated in Hartlepool by Zhong et al. (2025). This statistical downscaling approach is designed to establish empirical relationships between larger-scale atmospheric conditions (predictors) and local multivariate oceanographic variables (predictands). Given a statistically robust link between the predictors and predictands, weather typing can serve as an efficient alternative to dynamical downscaling (i.e., process-based dynamical modeling) while maintaining good accuracy. This section provides a brief introduction to weather typing, outlining the datasets involved and the main procedures.





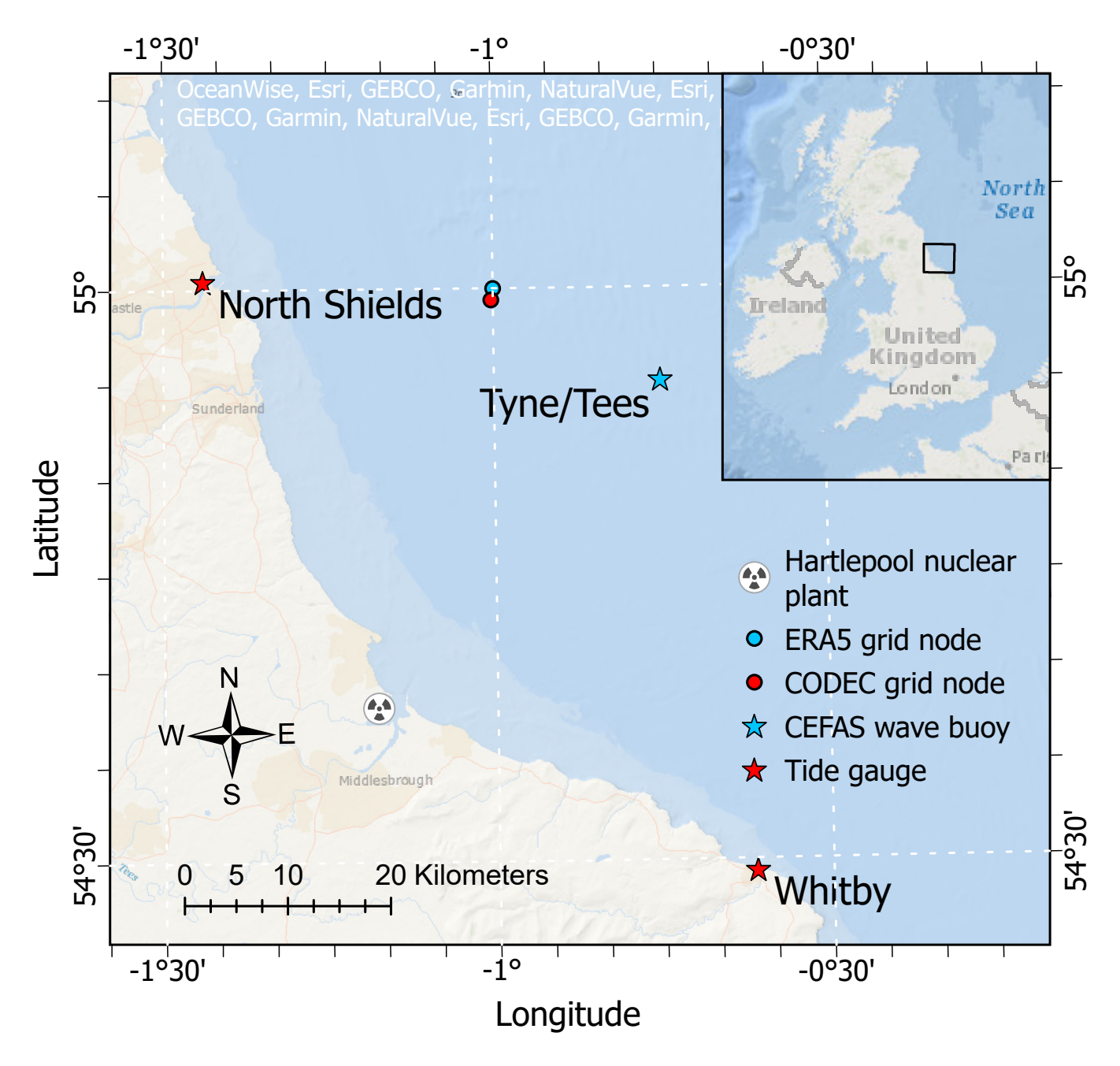


Figure 1. Locations of the nuclear station and data sources (Zhong et al., 2025).



100

105

120



Three types of data were used to derive the WTs. Large-scale atmospheric conditions were represented by sea level pressure (SLP) from ERA5, the fifth-generation global atmospheric reanalysis produced by the European Centre for Medium-Range Weather Forecasts (ECMWF) (Hersbach et al., 2020). The local wave climate conditions were also obtained from ERA5 at an offshore grid node near Hartlepool (55° N, 1° W; see Fig. 1). The wave node is around 24 km away from the coast and at a depth of 74 m. The wave climate conditions included hourly variables characterizing both the combined wind waves and swell (including significant wave height  $H_s$ , mean wave period  $T_m$ , peak wave period  $T_p$ , and mean wave direction  $\theta_m$ ) as well as individual wind wave and swell components (including significant height  $H_s^w$  and  $H_s^s$ , mean period  $T_m^w$  and  $T_m^s$ , and mean direction  $\theta_m^w$  and  $\theta_m^s$ , where the superscripts  $\theta_s^w$  and  $\theta_s^s$  denote wind wave and swell components, respectively). Storm surge (SS) conditions at a neighbouring location were obtained from CODEC (Muis et al., 2020), a global dataset for extreme sea levels and storm surges driven by wind and atmospheric pressure from ERA5. Validation of wave and storm surge was conducted in Zhong et al. (2025). In summary,  $H_s$  showed good agreement between ERA5 and the CEFAS wave buoy, whereas  $T_p$  displayed some discrepancies. SS from CODEC also compared well with those derived from tide gauges, although CODEC tends to slightly underestimate high surge values and overestimate low surge values. Consequently, a bias correction method was applied to SS. The weather typing analysis was conducted using data from 1979 to 2018.

The first step involved defining the atmospheric predictors in terms of variable selection, spatial domain, and temporal coverage. Here, the predictors were constructed from daily mean SLP and the squared SLP gradient (SLPG, which is closely related to the geostrophic winds) fields over a spatial domain extending from 26° N to 76° N and 40° W to 30° E, with a 2° spatial resolution. The predictors were averaged over 4 days to reflect the time scale typical for extratropical storms in the North Atlantic basin (Gulev et al., 2001; Haigh et al., 2016), which are the main drivers of wave climate and sea level variability in this region. To facilitate the classification of WTs, a Principal Component Analysis (PCA) was performed to reduce the dimensionality of the predictors while preserving 95 % of the data variance.

Next, a regression-guided classification (Camus et al., 2016) was implemented to categorize the predictors into a group of representative synoptic circulation patterns (i.e., weather types). This consisted of two key steps. First, a multivariate linear regression model was fitted between the predictors and a group of selected predictands (daily means of  $H_s$ ,  $T_p$ ,  $\theta_m$ , and daily maximum storm surge). The estimation from the regression model captured the synoptic-scale influence on the local sea states while filtering out irrelevant signals. Second, a semi-supervised clustering was performed on a dataset composed of the predictors and the estimated predictands from the regression model, with a weighting parameter introduced to control the relative contributions of the two components. The K-means clustering was then implemented to partition the dataset into 36 clusters, minimizing the total variance within a cluster. The cluster centroids were subsequently projected back into the original high-dimensional space and plotted in a 6-by-6 lattice, where clusters with lower centroid distances (i.e., higher similarity) are positioned closer together. Figure 2 displays the circulation patterns for 36 WTs, represented by the anomalies of SLP, as climate variability is typically analysed in terms of deviations from the climatology (Hurrell et al., 2003).

Once the WTs were defined, the relationships between predictors and predictands were established by collecting the predictands recorded on all dates when a specific WT occurred. This allowed for the derivation of empirical distributions of wave and storm surge variables associated with each WT. Model validation confirmed the effectiveness of WTs and their empirical





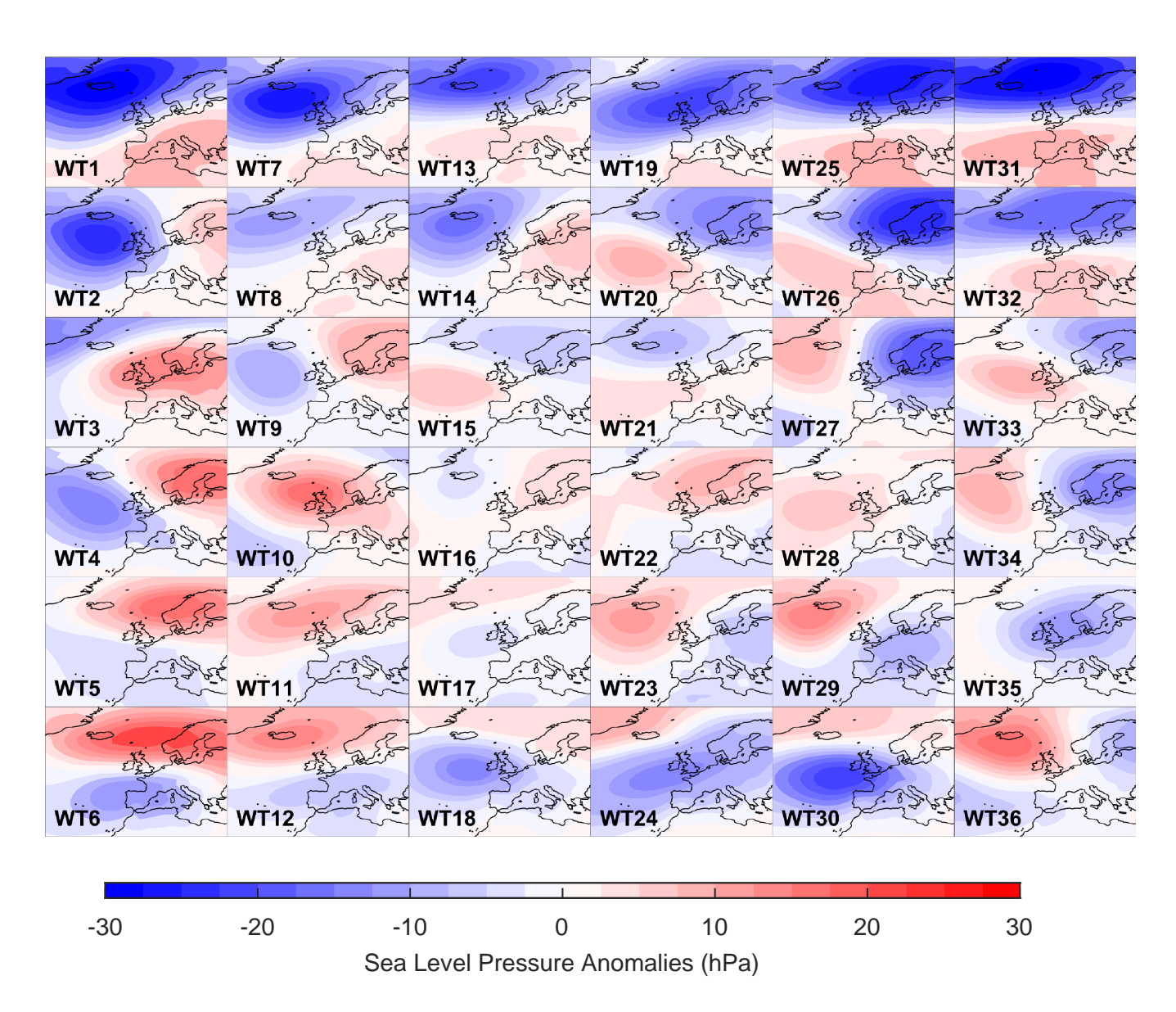


Figure 2. The synoptic circulation pattern of 36 WTs. The anomalies are calculated relative to the 1979–2018 mean SLP.



125



relationships in providing estimations of multivariate sea state variables with generally good accuracy and their limitation in reproducing wave direction and extreme wave events (Zhong et al., 2025).

Sensitivity analysis was conducted to investigate the impact of different model configurations on the performance of sea state downscaling. The analysis considered factors such as the choice of predictor variables, the spatial domain of the model, the number of days over which the predictors were averaged, the spatial resolution of the predictors, the number of WTs, and the weighting parameter used in the semi-supervised clustering. Some of the main findings are as follows: (1) using both SLP and SLPG as predictors outperforms using either one individually; (2) model performance shows low sensitivity to the spatial domain; (3) increasing the spatial resolution of the predictors does not significantly improve model performance; (4) increasing the number of WTs improves model performance, but more WTs means the associated sea state distributions for each individual WT are less representative. A detailed discussion is provided in Zhong et al. (2025).

## 2.2 Climate indices and their correlation with local sea state variability

The behaviour of climate oscillations is widely studied through climate indices, which are numerical representations of the phase and intensity of atmospheric or oceanic variability patterns. In this study, we examined six key climate indices: NAO, EA, SCAND, Arctic Oscillation (AO), East Atlantic Western Russian pattern (EA/WR), and WEPA. These are the main modes of climate variability over the North Atlantic and European regions and have been commonly considered in previous research (e.g., Martínez-Asensio et al., 2016; Hochet et al., 2021; Scott et al., 2021).

The first five indices were obtained from the National Oceanic and Atmospheric Administration (NOAA) Climate Prediction

140 Center. They were calculated using Rotated Principal Component Analysis (Barnston and Livezey, 1987), applied to monthly

mean standardized 500 mb height anomalies in the Northern Hemisphere (20°–90° N). The WEPA index, available at Scott

et al. (2020), was developed in Castelle et al. (2017) to explain the variability of winter wave activity along the Atlantic coast

of Europe. Its definition is based on the normalized SLP difference between the stations Valentia (Ireland) and Santa Cruz de

Tenerife (Canary Islands).

A correlation analysis was conducted using these six climate indices to identify climate oscillations relevant to wave climate and storm surge variability at Hartlepool. The analysis focuses on the extended winter months (December to March, DJFM), which aligns with previous research (e.g., Martínez-Asensio et al., 2016; Scott et al., 2021). This is the period when the atmospheric pressure in the Northern Hemisphere exhibits the greatest variability and perturbations reach their largest amplitudes, significantly influencing local wind fields, wave climate, and sea levels (Hurrell et al., 2003; Shimura et al., 2013).

By contrast, during summer, when westerlies and extratropical storms are weaker, mesoscale processes become more relevant in determining local wave characteristics, particularly in coastal areas (Semedo et al., 2015).

First, we calculated the mean climate indices, the mean wave variables (including the combined wind waves and swell as well as individual wind wave and swell components), the 99th percentile of  $H_s$  ( $H_{s99}$ ), and the 1st, 50th, and 99th percentiles of SS ( $SS_1$ ,  $SS_{50}$ , and  $SS_{99}$ ) in each DJFM period. Next, Kendall's  $\tau$  coefficient was calculated to measure the correlation for scalar quantities (i.e., storm surge, wave height, and wave period). We selected this measure of correlation because it does not require variables to be normally distributed (which is the assumption for the Pearson correlation) and is less sensitive to



165

170

180

185



outliers than Spearman's  $\rho$ . For circular variables (wave direction), we used a circular–linear correlation method described in Berens (2009). The correlation coefficient  $\rho_{cl}$  between a liner variable x and a circular variable  $\theta$  is defined as:

$$\rho_{cl} = \sqrt{\frac{\rho_{cx}^2 + \rho_{sx}^2 - 2\rho_{cx}\rho_{sx}\rho_{sc}}{1 - \rho_{sc}^2}},\tag{1}$$

where  $\rho_{sx} = \text{corr}(\sin \theta, x)$ ,  $\rho_{cx} = \text{corr}(\cos \theta, x)$ ,  $\rho_{sc} = \text{corr}(\sin \theta, \cos \theta)$ , and corr() denotes the Pearson correlation coefficient. The range of  $\rho_{cl}$  is between 0 and 1, with greater values indicating stronger association between x and  $\theta$ .

#### 2.3 Associating WTs with climate oscillations

The synoptic circulation patterns of certain WTs have similar structures to some climate oscillation patterns. For example, WT31 is characterized by strong negative pressure anomalies over Iceland and the Norwegian Sea and positive pressure anomalies across mid-latitudes (Fig. 2). This pattern closely resembles the spatial structure of the positive phase of NAO, which indicates a potential link. However, not all WTs have distinct spatial patterns, and some WTs may reflect the influence of multiple overlapping climate modes.

To establish a more general and robust link between WTs and climate oscillations, we calculated the percentage of WT occurrence under a positive or negative index during DJFM. A WT was associated with a specific climate phase if its occurrence probability under that phase exceeded a threshold  $(P_i)$ , which was set to 60 %. For instance, WT1 was classified under positive NAO because 89 % of its occurrence coincided with a positive NAO index, compared to just 11 % with a negative index. The occurrence percentage naturally served as an indicator of the strength of this association. The selection of this threshold was subjective, and the choice of 60 % was intentionally conservative to ensure that each climate phase was associated with a larger set of WTs. Additionally, WTs with a low occurrence frequency during DJFM  $(P_w)$  were excluded from the categorization to maintain statistical robustness in the association. We used a threshold of 1.5 % for  $P_w$ . The results are listed in Table B1 and visualized in Fig. 3. A sensitivity analysis was conducted on the values of  $P_i$  (i.e., 60 %, 65 %, 70 %) and  $P_w$  (i.e., 1.5 %, 2 %, 2.5 %) to examine the robustness of this approach.

## 2.4 Parametrization of atmospheric processes

Climate oscillations influence sea states by modifying atmospheric circulation, such as wind and storm patterns. To understand the role these individual processes play in the connection between climate oscillation and sea state variability, we parametrized their effects on wave climate and storm surge. For each atmospheric process, we identified the key parameters that represent its intensity and related them to sea states conditions. It should be noted that the explicit physical mechanisms underlying air—sea interactions are complex and beyond the scope of this research.

The wave climate is dependent on the effects of local wind and distant storms. Gulev and Grigorieva (2006) performed a Canonical Correlation Analysis over the North Atlantic and North Pacific and found that wind wave variability is closely linked to local wind speed, whereas swell is more strongly associated with the frequency of deep (< 980 hPa) cyclones. To parametrize the impact of local wind, we obtained the surface wind speed W from ERA5 using the eastward and northward



190

195



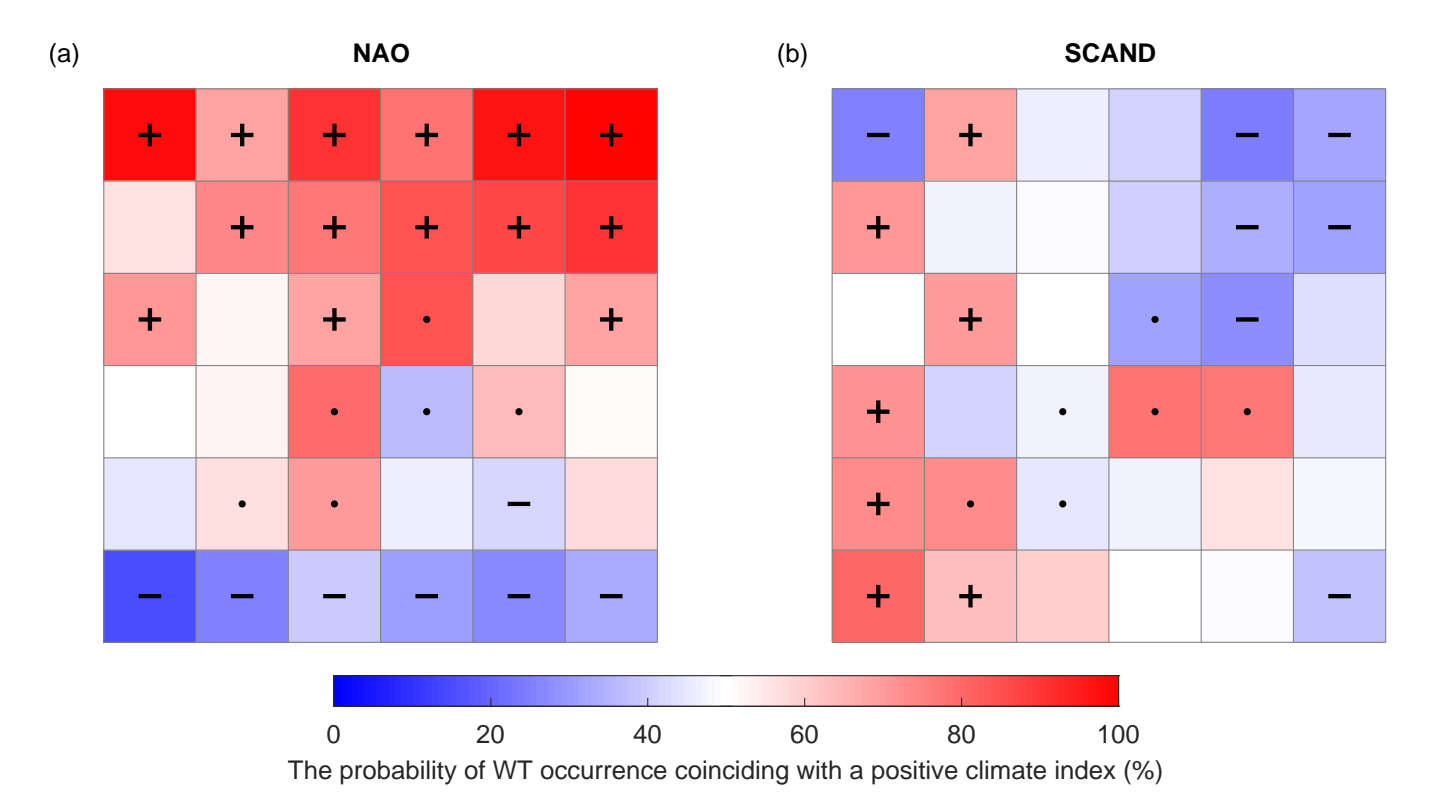


Figure 3. Percentage of WT occurrence coinciding with a positive climate index during DJFM. Each cell in the  $6 \times 6$  lattice corresponds to the WT of the same location in Fig. 2. WTs are marked with a plus sign (+) if classified in the positive phase, a minus sign (-) if in the negative phase, or a dot if excluded from the classification due to low occurrence frequency during DJFM (based on the  $P_w$  threshold).

10 m wind components (U and V, respectively). The wind speed was averaged over a  $0.5^{\circ} \times 0.5^{\circ}$  grid box centred on the study location to represent regional wind conditions. For the impact of extratropical storms on waves, we used the storm track dataset derived in Camus et al. (2024). The dataset was generated by applying a storm tracking algorithm to sea level pressure and 10 m wind speed fields at  $0.25^{\circ}$  resolution from ERA5. The algorithm calculated the vortex strength based on the U and V wind components and identified potentially significant storms by applying both a vortex strength threshold (0.5) and a sea level pressure threshold (1010 hPa) on an hourly basis. Once a storm was detected, it was tracked over consecutive time steps using a nearest neighbour detection approach within a maximum distance of  $5^{\circ}$ . The storm frequency was parametrized by the number of hours with storms detected in each  $1^{\circ} \times 1^{\circ}$  grid box divided by the total number of hours.

Storm surges are mainly driven by changes in the atmospheric pressure and the force of wind stress (Pugh and Woodworth, 2014). The impact of atmospheric pressure is commonly known as the inverse barometer effect, which is expressed as:

$$\Delta \zeta = -\Delta P_A / \rho g,\tag{2}$$





where  $\Delta \zeta$  is the change in sea level,  $\Delta P_A$  is the local pressure anomaly relative to the global mean sea level pressure over the entire ocean (assumed to be constant at 1013.3 hPa in most applications),  $\rho$  is water density, and g is the gravitational acceleration (Pugh and Woodworth, 2014). Hence, the impact of atmospheric pressure on storm surge was parametrized by  $\Delta P_A$ . Since each WT is represented by a spatial pattern of SLP, the  $\Delta P_A$  at our study location (55° N, 1° W) was estimated by SLP values on the four nearest grid points. These values were averaged with a weight of the cosine of the corresponding latitude to account for the convergence of meridians at higher latitudes. Storm surge generated by wind occurs through the shear stress exerted by wind on the sea surface, which pushes water toward certain directions. In shallow waters, the storm surge caused by wind stress can be expressed in the following form:

$$\frac{\partial \zeta}{\partial x} = \frac{\rho_{\text{air}} C_d W^2}{\rho g D},\tag{3}$$

where  $\frac{\partial \zeta}{\partial x}$  is the gradient of sea level,  $\rho_{\rm air}$  is air density,  $C_d$  is the drag coefficient (related to wind speed due to increasing roughness of sea surface with a stronger wind), W is wind speed, and D is water depth (Pugh and Woodworth, 2014). Since our focus is on representing the effect of wind stress on storm surge rather than quantifying wind-generated surge itself, we parametrized this effect using W only.

## 3 Results

210

#### 3.1 Correlations between climate indices and local sea states

The first objective of the study is to identify climate oscillation patterns contributing to the sea state variability at Hartlepool.

This was achieved through a correlation analysis between six climate indices and local wave and storm surge variables, with the results given in Table 1. Significant correlations (at 95 % confidence interval) are found for NAO, AO, SCAND, and WEPA, with moderate to strong associations. NAO and AO show similar correlation patterns, particularly for storm surge and wave directions. This is not surprising considering the strong correlation between these two indices, with a Pearson coefficient of 0.80 between their winter means. Indeed, there has been ongoing debate about whether they represent distinct phenomena or different manifestations of the same underlying climate variability (e.g., Ambaum et al., 2001; Itoh, 2008). SCAND seems to have the opposite correlation compared to NAO. No significant correlation is found for either EA or EA/WR.

Although four indices were identified as relevant to local sea state variability, we focus on NAO and SCAND for further analysis based on the following considerations. The subtle differences between NAO and AO are unlikely to be distinguished by our WTs which only account for the Atlantic region. NAO is chosen as it has been extensively examined in previous studies and may provide a more physically meaningful interpretation of climate dynamics than AO (Ambaum et al., 2001). WEPA is not considered because it is more relevant in regions southwards of 52° N (Castelle et al., 2017, 2018; Scott et al., 2021).





**Table 1.** Correlation coefficients between winter sea state parameters and winter mean index values. Kendall's  $\tau$  coefficient was used for wave height, wave period, and storm surge variables, while a circular-linear correlation (Berens, 2009) was calculated for circular variables  $(\theta_m, \theta_m^w, \text{ and } \theta_m^s)$ . Bold values indicate statistical significance (p-value < 0.05). The analysis was conducted for the period 1979–2018.

	NAO	AO	SCAND	EA	EA/WR	WEPA
$H_s$	-0.08	-0.37	0.17	0.01	-0.18	0.31
$H_{s99}$	-0.10	-0.24	0.17	0.06	0.07	0.12
$T_m$	-0.38	-0.45	0.25	-0.07	-0.10	-0.07
$T_p$	-0.29	-0.27	0.11	0.01	0.01	-0.21
$H_m^w$	0.31	0.09	-0.16	-0.01	-0.10	0.26
$T_m^w$	0.22	0.01	-0.09	-0.01	-0.09	0.30
$H_m^s$	-0.41	-0.65	0.40	-0.03	-0.17	0.20
$T_m^s$	-0.01	-0.16	-0.03	-0.02	-0.02	-0.08
$\theta_m$	0.63	0.75	0.69	0.37	0.23	0.53
$ heta_m^w$	0.74	0.71	0.66	0.30	0.09	0.45
$\theta_m^s$	0.61	0.53	0.52	0.38	0.26	0.53
$SS_1$	-0.15	0.00	-0.11	0.06	-0.08	0.06
$SS_{50}$	0.36	0.29	-0.45	0.19	-0.10	0.25
$SS_{99}$	0.62	0.63	-0.48	-0.06	0.09	-0.12

## 3.2 The response of sea states to climate indices

The second objective of the study is to characterize the response patterns of wave and storm surge to the selected climate oscillations. The 36 WTs, along with their empirical distributions of wave climate and storm surge, were associated with the positive or negative phases of NAO (NAO+, NAO-) and SCAND (SCAND+, SCAND-). The categorization of each WT is shown in Fig. 3. WTs associated with NAO+ and NAO- are found at the top and bottom of the lattice, while those associated with SCAND+ and SCAND- are mainly positioned on the left and right sides, respectively. It should be noted that the positioning of each WT is purely based on the centroid distances (i.e., similarity of their spatial patterns) between its neighbouring WTs and doesn't consider which climate phases they are associated with. The reason that most WTs associated with the same climate phase are placed together is that they share more or less the same broad-scale atmospheric circulation structure. This section focuses on identifying common response patterns linked to the same climate phase and comparing the differences between the positive and negative phases.

#### 3.2.1 Wave climate

230

235

240

The response of wave climate is complicated due to its multivariate nature. For the combined wind waves and swell, distinct patterns emerge in  $T_p$ . For WTs associated with NAO+ (Fig. 4a), the individual  $T_p$  distributions typically take two forms: a unimodal distribution with a high peak around 4–6 s and a long tail to the right, or a bimodal distribution with peaks at





245

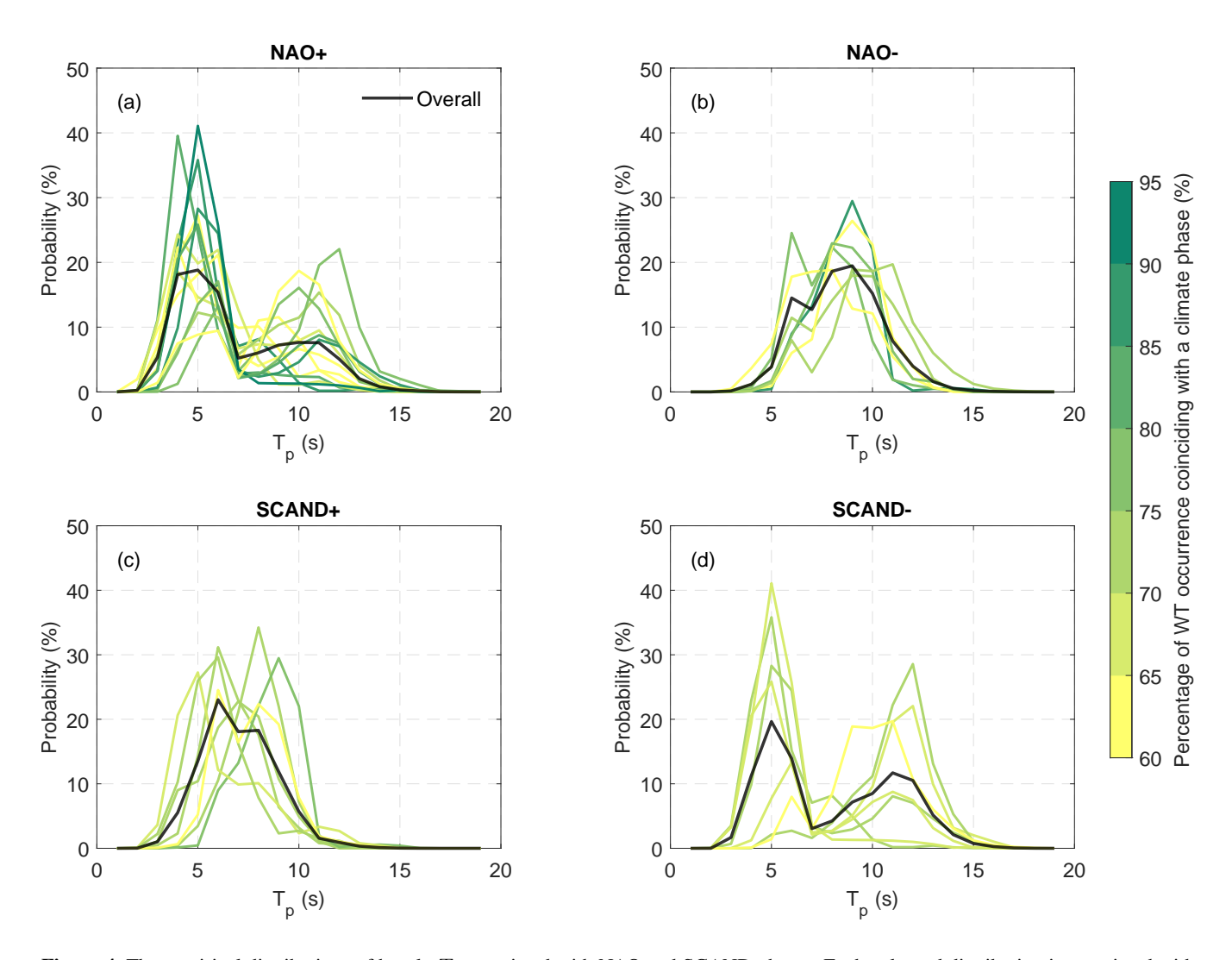


Figure 4. The empirical distributions of hourly  $T_p$  associated with NAO and SCAND phases. Each coloured distribution is associated with an individual WT, with the colour representing the percentage of WT occurrence in particular phases of climate mode in Table B1, thus indicating the strength of the association. The overall distributions (black) are derived from the storm surge related to all WTs under the same category.

4–6 s and 10–12 s. As a result, the overall  $T_p$  distribution for all WTs linked to NAO+ is bimodal, with the left peak being more pronounced than the right. In contrast, WTs associated with NAO- do not exhibit two distinct modes in the overall  $T_p$  distribution, which is closer to a unimodal distribution with a broad peak spanning across 5–10 s (Fig. 4b). The pattern observed for SCAND- closely resembles that of NAO+, while the distributions related to SCAND+ are also similar to those seen for NAO- (Fig. 4c and 4d). These patterns are not observed in the  $T_m$  distributions (Fig. A1).



250

255

260



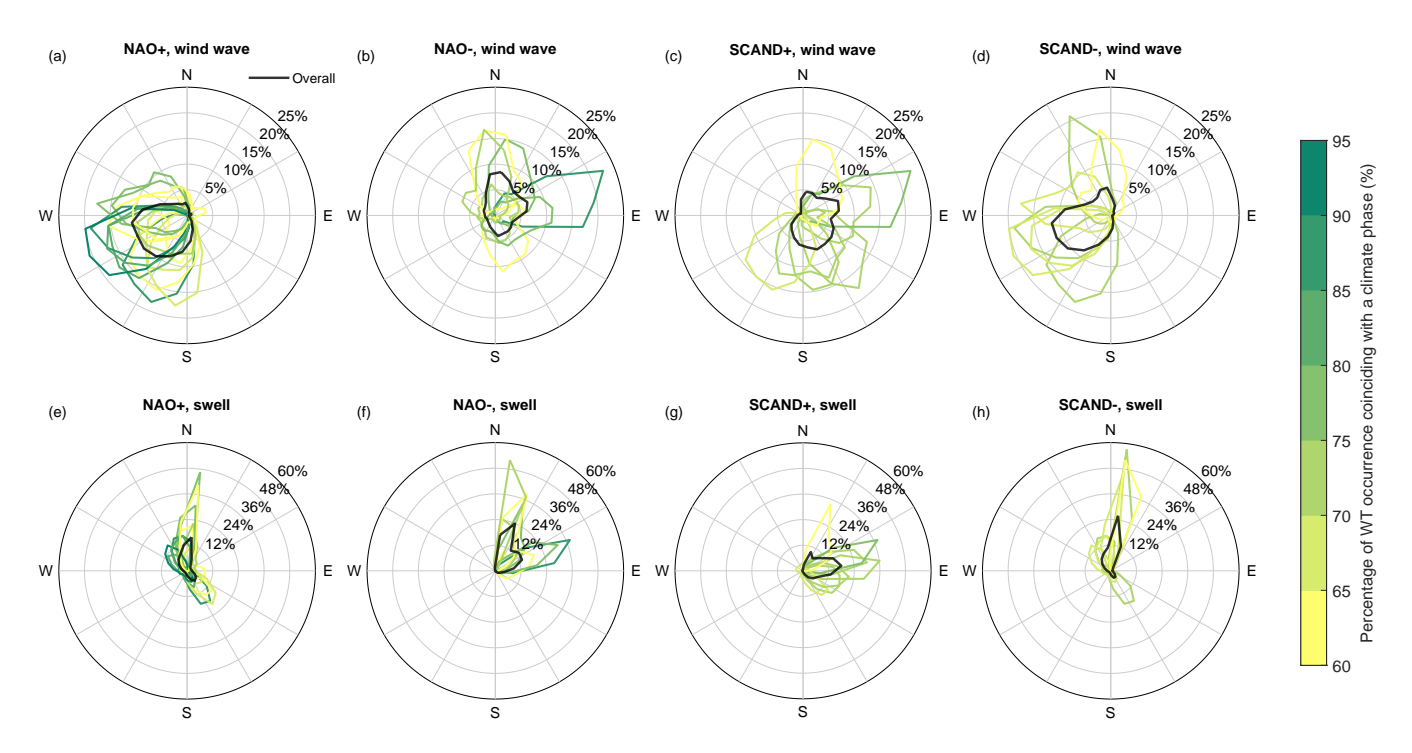


**Figure 5.** The empirical distributions of hourly  $\theta_m^w$  and  $\theta_m^s$  associated with NAO and SCAND phases (similar to Fig. 4). The radial axis indicates the percentage of wave travelling from each 15° directional bin.

The two modes in  $T_p$  represent the wind waves and swell respectively, which display different patterns in response to NAO/SCAND. For WTs associated with NAO+, the overall  $\theta_m^w$  distribution primarily spans between south and west, with the individual distributions for each WT also generally falling within the same range (Fig. 5a). These south-westerly wind waves have similar wave height distributions, with most measuring less than 1 m (Fig. 6a). Swell waves, on the other hand, are primarily from two distinct directions: north and south-east. The northerly waves are observed with higher frequency and larger magnitudes (Fig. 5e and 6e). For WTs associated with NAO-, the overall  $\theta_m^w$  distribution essentially flips to the opposite side compared to the positive phase, spanning from north to east and somewhat extending into the south (Fig. 5b). The individual  $\theta_m^w$  distributions exhibit more variability than those of NAO+. Unlike  $\theta_m^w$ ,  $\theta_m^s$  shows more consistency among WTs, with the overall distribution displaying two peaks between north and east (Fig. 5f). Concerning wave height related to NAO-, swell waves are generally larger than wind waves. In fact, most of these swell waves are also larger than those related to NAO+ (Table B2).

For WTs related to SCAND+, the overall  $\theta_m^w$  distribution mainly extends from north to south, covering the eastern half of the wave rose (Fig. 5c). These wind waves are relatively small in height, averaging only 0.79 m (Table B2). In comparison, swell waves are more concentrated in the east and have greater wave heights (Fig. 5g and 6g). Regarding WTs associated with SCAND-, we also observe a flip in the overall  $\theta_m^w$  distribution (Fig. 5d) compared to that of SCAND+. Wind waves now dominate the western half of the wave rose, with the majority of them coming from the south-west. Meanwhile, most swell





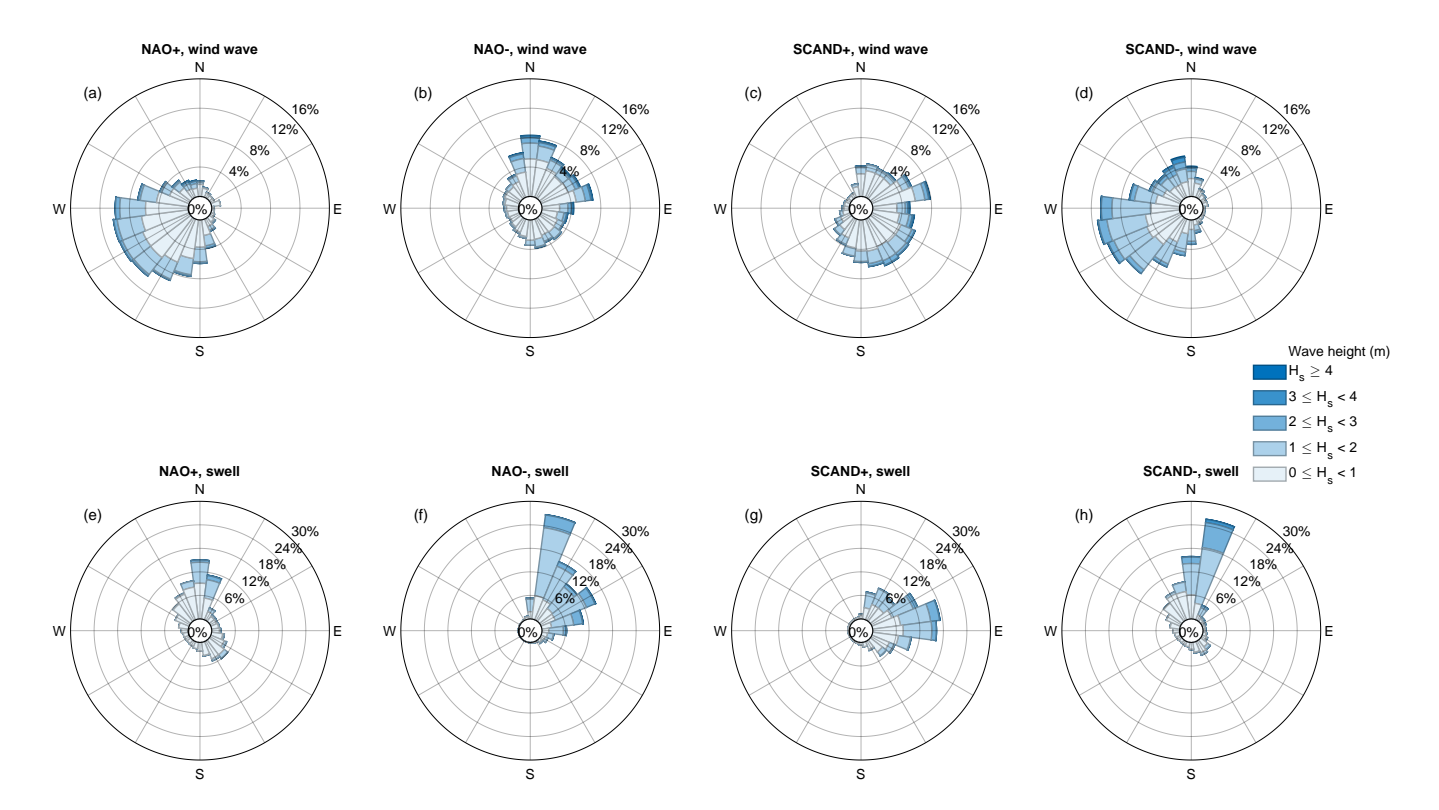


**Figure 6.** The wave rose diagrams for wind waves and swell associated with NAO and SCAND phases. Each diagram represent the overall wave distribution of all WTs associated with the same climate phase. In addition to directional distribution (as in Fig. 5), the diagrams also show the wave height distribution (indicated by the colour) in each 15° directional bin.

waves travel from a much narrower range in the north (Fig. 5h). In this case,  $H_s^w$  and  $H_s^s$  are more comparable, with a mean of 1.16 m and 1.05 m respectively (Table B2).

Table B2 also shows the probability of  $H_s^w$  being higher or lower than  $H_s^s$ . Since wave energy is proportional to the square of wave height, this also indicates the likelihood of wind waves or swell dominating the wave energy spectra. Under WTs related to NAO+/SCAND-, wind wave dominance is slightly more frequent than swell dominance. Conversely, for NAO-/SCAND+, the wave field is more likely to be dominated by swell.

#### 3.2.2 Storm surge

Storm surge distributions for individual WTs typically resemble a normal distribution, but their characteristics (e.g., relative position and spread) vary significantly depending on their association with climate modes. For WTs linked with NAO+ (Fig. 7a), most distributions tend to shift toward more positive values, meaning that there's a higher proportion of positive surges compared to negative ones. This positive shift is more pronounced for WTs with a higher occurrence percentage when the NAO index is positive (i.e., WTs more strongly associated with NAO+). In addition, WTs with a stronger association tend to have





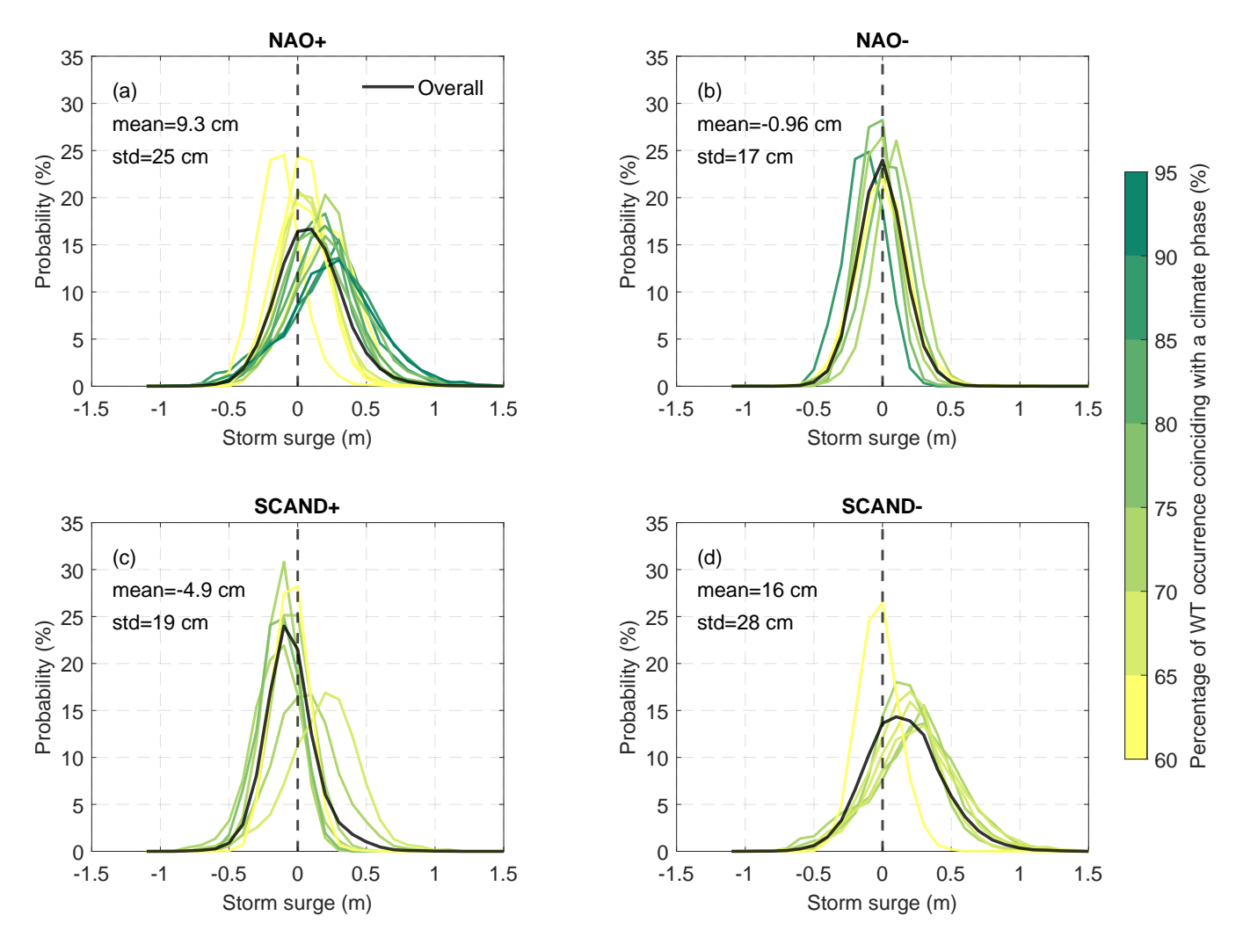


**Figure 7.** The empirical distributions of hourly storm surge magnitude associated with the positive and negative phases of NAO and SCAND (similar to Fig. 4). The means and standard deviations of the overall distributions are provided.

lower and wider peaks, indicating a greater spread in storm surge values. In contrast, for NAO- (Fig. 7b), the distributions generally have a high and narrow peak centred around 0 m. These characteristics can be parametrized by the mean ( $\mu_{SS}$ ) and standard deviation ( $\sigma_{SS}$ ): the overall storm surge distribution associated with NAO+ has both a higher  $\mu_{SS}$  and a greater  $\sigma_{SS}$  than that of NAO-. Similar patterns are also observed regarding the response to SCAND. The surge distributions related to SCAND- (Fig. 7c) tend to shift to the positive side (positive  $\mu_{SS}$ ) and have lower and broader peaks (higher  $\sigma_{SS}$ ) compared to WTs related to SCAND+ (Fig. 7d). It is worth noting that, although some WTs deviate from the general pattern observed within their group, their association with the corresponding climate mode is relatively weaker.



285

290

305

310



## 3.2.3 Sensitivity analysis

The response patterns identified previously may be sensitive to the choice of thresholds ( $P_w$  and  $P_i$ ) applied in linking WTs to climate oscillation phases. Hence, we performed a sensitivity analysis to assess how they influence the relationships between key characteristics of sea state conditions and climate oscillations (Table B3). Despite the variations in statistics, the following patterns remain consistent across all tested cases: (1) mean  $H_s^w$  is higher under SCAND+ than SCAND-; (2) mean  $H_s^s$  is higher in NAO- than NAO+, but it remains more or less at 1 m in both phases of SCAND; (3) the wave energy spectra are more frequently dominated by wind waves during NAO+/SCAND- and by swell during NAO-/SCAND+; (4) both  $\mu_{SS}$  and  $\sigma_{SS}$  related to NAO+/SCAND- are higher than those linked to NAO-/SCAND+. It is worth noting that as the statistical association between WTs and climate phases strengthens (i.e., higher  $P_w$  or  $P_i$ ),  $H_s^w$  shows an increasing difference between the two phases of NAO (from 0.04 m to 0.13 m or 0.32 m, respectively).

Moreover, the sensitivity of wave direction to  $P_w$  and  $P_i$  was tested (Fig. A2 and A3). Overall, the distribution of wave direction is insensitive to these two thresholds, with the exception of the NAO- category, which exhibits noticeable variation as  $P_w$  increases.

#### 295 3.3 Processes contributing to variabilities of wave climate and storm surge

The third objective of this study is to investigate the atmospheric processes linking climate oscillations to the corresponding sea state responses. This may offer insights into the physical mechanisms by which climate oscillations contribute to sea state variability. In this section, the atmospheric processes are examined through the lens of wind forcing, storm frequency, and atmospheric pressure anomaly.

#### **300 3.3.1 Wave climate**

First, the link between wind forcing and wind wave pattern is examined. We derived the wind pattern associated with NAO and SCAND based on the categorization of WTs (Fig. 8). The wind directions related to NAO+ and SCAND- are concentrated in the south-west, which is consistent with the corresponding  $\theta_m^w$  distributions (Fig. 6). On the other hand, the wind directions during NAO-/SCAND+ are more broadly distributed but still align well with the wind wave patterns. Apart from direction, the mean local wind speed W is very well correlated with the corresponding mean  $H_s^w$  for each WT, irrespective of the climate phases, with a correlation coefficient of 0.95.

Next, we explored the possibility of relating swell wave variability to extratropical storm activity. Figure 9 illustrates the spatial distribution of storm occurrence frequency associated with different climate phases. We only focus on the region where swell waves can propagate to our study site, which was estimated by assuming that deep water waves propagate along great circle paths (Pérez et al., 2014). Areas where these paths to the study site are clearly blocked by land were excluded. The resulting source region covers the North Sea and much of the Norwegian Sea. During NAO+/SCAND-, the Norwegian Sea experiences more frequent storms than the North Sea. This pattern is consistent with the corresponding swell wave conditions, where waves predominantly come from the north with higher wave heights. During NAO-, the storm activity shifts toward





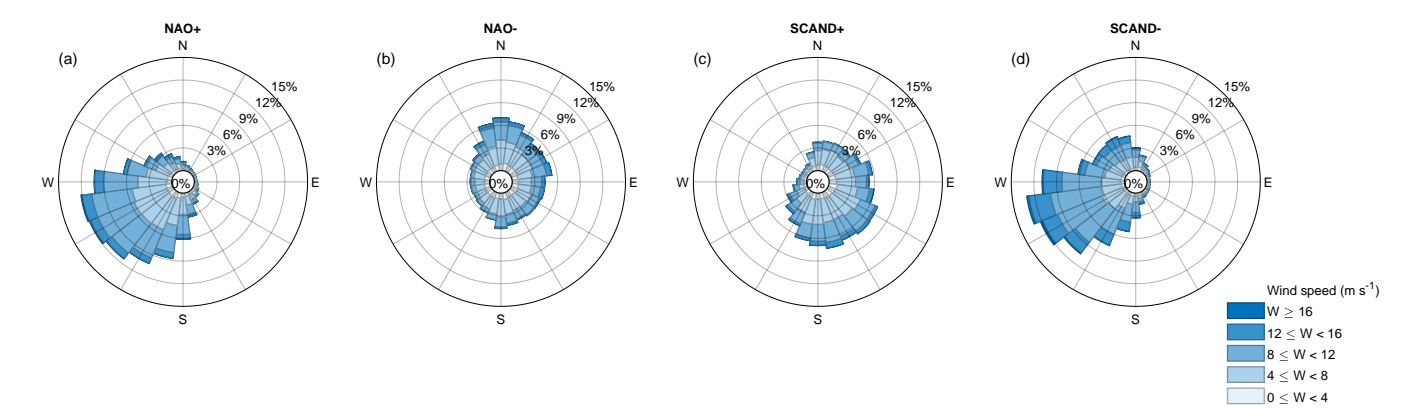


**Figure 8.** Wind rose diagrams associated with NAO and SCAND phases, showing the distribution of wind directions (indicating where the wind blows from, consistent with the wave directions) and corresponding wind speeds, similar to Fig. 6. Wind conditions are represented by the regional weighted mean over a  $0.5^{\circ} \times 0.5^{\circ}$  grid box centred on the study location.

the North Sea and the southeastern Norwegian Sea. This pattern corresponds with swell waves propagating from more easterly directions. The storm frequency in SCAND+ is lower than the other three cases, but the regions with relatively higher density (the southern North Sea) generally align with the dominant swell direction.

It is worth noting that the travel time of swell waves from their source regions to the study site is not accounted for in our analysis. As a result, the WT associated with a storm may differ from the WT associated with the resulting swell, which can arrive several days later. To assess the impact of this limitation, we also categorized the storms based on the monthly indices (i.e., independent of WTs) and calculated the spatial distribution of storm frequency for each climate phase (Fig. A4). Months in which the index exceeded 1 standard deviation were classified as being in the positive phase, while those below -1 standard deviation were considered in the negative phase. As can be seen, no substantial differences in storm spatial patterns are observed between the two approaches across all climate phases, suggesting that neglecting swell travel time does not influence our findings.

#### 3.3.2 Storm surge

320

325

330

The response pattern of storm surge mainly lies in the position and shape of the storm surge distributions, which can be represented by  $\mu_{SS}$  and  $\sigma_{SS}$ , respectively. To investigate the underlying drivers, a correlation analysis was performed between these distribution parameters and the effects of atmospheric processes (see Table 2). We found a strong correlation between  $\mu_{SS}$  and the effects of both atmospheric pressure and wind stress. Among the wind parameters we considered, U displays the strongest correlation (0.83) while V is not significantly correlated. In addition, we calculated the storm surge caused by atmospheric pressure anomaly ( $\Delta\zeta$  in Eq. (2)) for each WT and compared it with the  $\mu_{SS}$  of each storm surge distribution, with the Root Mean Square Deviation (RMSD) and BIAS provided (Fig. A5). Their definitions are given as follows:





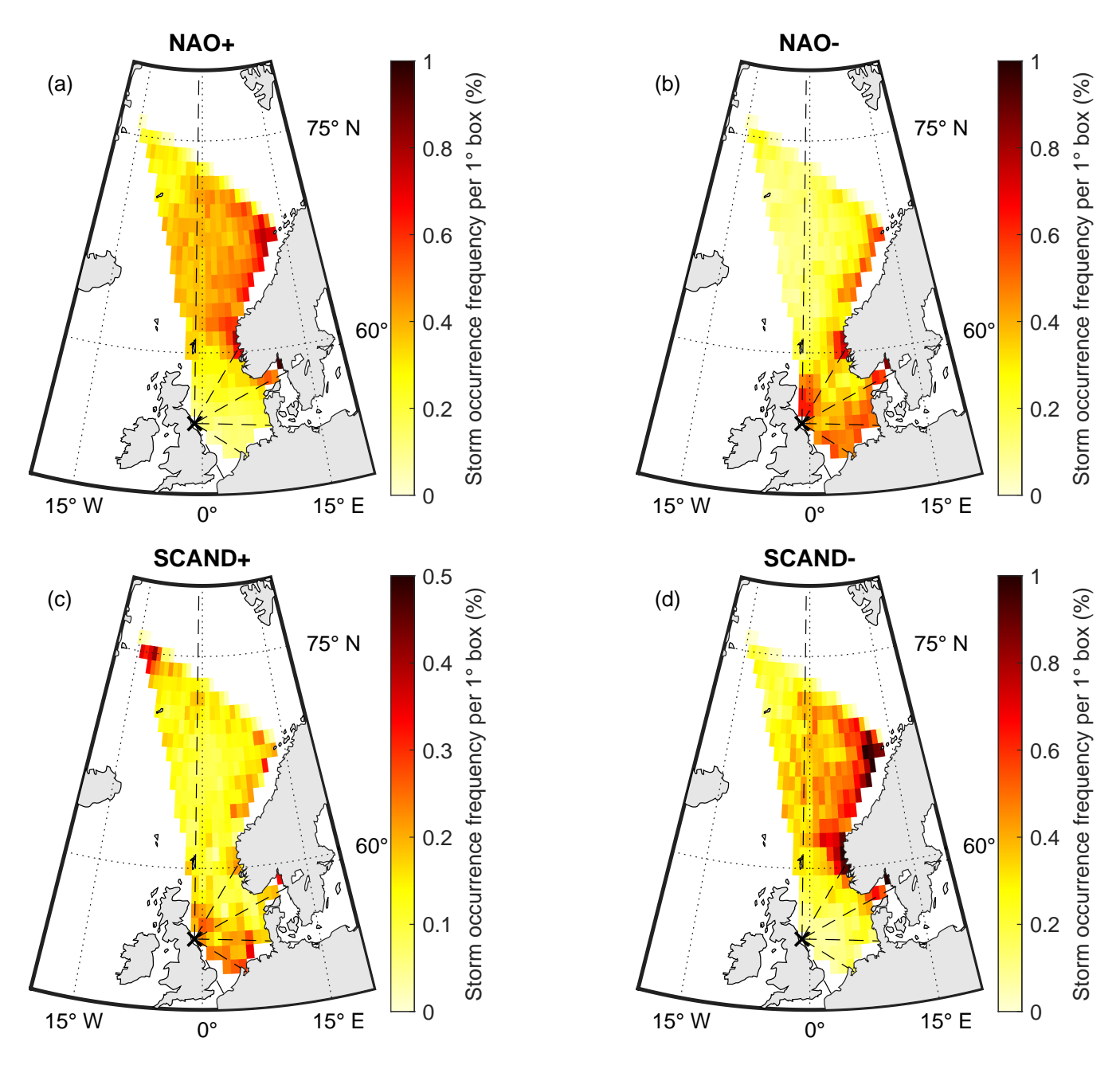


**Figure 9.** Spatial distribution of storm occurrence frequency associated with NAO and SCAND phases. For each  $1^{\circ} \times 1^{\circ}$  grid box, the frequency is calculated by the number of hours with storms detected divided by the total number of hours. The association of storm tracks with climate phases is based on the WT categorization. The black cross indicates the study location. Radial black dashed lines originating from the study site indicate great circle paths at  $30^{\circ}$  intervals. Note that panel (c) uses a smaller colour-bar range than the others.





**Table 2.** Pearson correlation coefficient between storm surge parameters related to each WT and parametrizations of atmospheric processes. Bold values indicate statistical significance (p-value < 0.05).

	$-\Delta P_A$	U	V	W	$W^2$
$\mu_{SS}$	0.80	0.83	0.27	0.75	0.76
$\sigma_{SS}$	0.64	0.69	0.38	0.91	0.93

$$RMSD = \sqrt{\frac{\sum_{i=1}^{n} (x_i - y_i)^2}{n}},$$
(4)

BIAS = 
$$\frac{1}{n} \sum_{i=1}^{n} (x_i - y_i),$$
 (5)

where x and y are a pair of random variables, n is the number of variable pair (equals the number of WTs). The result shows a good agreement, with the RMSD and BIAS being 7.19 cm and 1.57 cm, respectively. For  $\sigma_{SS}$ , the strongest correlation is found with  $W^2$  (0.93).

#### 4 Discussion

In this work, we investigated the link between large-scale climate oscillations and local wave climate and storm surge through WTs. We focused on two key climate indices, NAO and SCAND, as our correlation analysis revealed their association with local sea state variables. These two climate indices were also widely considered in previous research on the sea state variability in the North Sea or the wider North Atlantic region. For instance, Frederikse and Gerkema (2018) developed multivariate linear regression models using the three leading principal components (PCs) of SLP to explain seasonal sea level deviation. They found that the PCs related to NAO and SCAND were primarily responsible for the variance explained by the model at North Shields, a tide gauge station near our study location. For wave climate, Shimura et al. (2013), Hochet et al. (2021), and Casas-Prat et al. (2024) showed the variability of  $H_s$  in the North Sea was associated with NAO and SCAND among other climate indices. Although our correlation analysis did not show significant associations between these two indices and  $H_s$ , other wave variables were found to be linked to NAO and SCAND. The impacts of these climate oscillations on wave climate and storm surge are further elucidated through our WT-based analysis.

#### 350 4.1 The link between climate oscillations and wave climate

The relationship between ocean waves and climate oscillations has been widely discussed in previous studies, with a focus on  $H_s$ . A commonly observed pattern in the North Atlantic basin is that  $H_s$  tends to be positively correlated with the NAO index at higher latitudes, while showing a negative correlation at mid-latitudes (Shimura et al., 2013; Hochet et al., 2021). However, in



355

360

365

370

375

380

385



the North Sea where the basin is more sheltered from the open ocean, the association between  $H_s$  and NAO is notably weaker, with the correlation in winter generally below 0.5 (Semedo et al., 2015). In our study, no significant link was found between  $H_s$  and NAO or SCAND through either correlation analysis (Table 1) or comparing the  $H_s$  distributions associated with each climate phase (not shown). Nevertheless, the link climate oscillations and local wave climate is reflected in the patterns of  $T_p$  and characteristics of wind wave and swell.

First, we observed that local  $T_p$  distributions are bimodal during NAO+/SCAND— and near-unimodal shapes during NAO-/SCAND+. This pattern is likely attributable to the frequency of observing wind wave-dominated or swell-dominated wave spectra. During NAO+/SCAND—, the chance of the wave spectra at Hartlepool being dominated by either wind waves or swell is relatively comparable (around 56 % and 44 %, respectively), which leads to the formation of two distinct peaks in  $T_p$  distributions. On the other hand, during NAO-/SCAND+, the wave spectra are largely dominated by swell, resulting in a low probability of  $T_p$  falling in the wind wave range, which is insufficient to form a distinct secondary peak. This wave climate characteristic is different from the general pattern in the global open ocean, where the prevalence of swell is observed almost everywhere, even in mid to high latitudes along the extratropical storm tracks (Semedo et al., 2011). Our results suggest that the likelihood of wind wave dominance can exceed that of swell waves in more sheltered areas under NAO+/SCAND—. Semedo et al. (2015) also reported a lower frequency of swell-dominated wave fields in this region under NAO+, consistent with our findings.

Beyond the relative dominance of wind waves or swell, the wave directions are also affected by climate phases. The prevailing wind conditions under NAO+/SCAND- closely align with the primary wind wave directions, and this relationship remains robust throughout our sensitivity analyses. In contrast, during NAO-/SCAND+, local wind directions show greater variability and do not fully align with the corresponding wind wave directions. In addition, both the wind and wind wave patterns under NAO-/SCAND+ show some sensitivity to the criterion used to define the climate phases. These suggest that the relationships between climate oscillations and wind waves are weaker and less robust in these scenarios. One possible explanation is that when large-scale westerly winds are suppressed, mesoscale processes (e.g., sea breezes or coastal low-level jet) may play a more significant role in driving local wind wave variability (Semedo et al., 2015). For swell waves, the dominant directions generally correspond to the regions with higher storm frequency in each climate phase. Gulev and Grigorieva (2006) further suggested that swell wave height is related to storm frequency. However, our results do not support this relationship — the mean  $H_s^s$  is higher in NAO- compared to NAO+, but the overall storm frequency in the Norwegian Sea and the North Sea does not follow a similar trend. This discrepancy suggests that other factors, such as storm intensity, duration, and the size of the effective fetch area, may be more relevant in determining  $H_s^s$  variability.

#### 4.2 The link between climate oscillations and storm surge

Storm surge characteristics in the North Sea generally display a positive correlation with the NAO index, with this association being stronger in the northeastern part of the basin, as revealed by previous research (e.g., Wakelin et al., 2003; Woodworth et al., 2007). Woodworth et al. (2007) further showed that the sensitivity to NAO differs between median and extreme storm surge conditions:  $SS_{99}$  increases more than  $SS_{50}$  for each unit increase in the NAO index. This difference in sensitivity can



390

395

420



be explained by the change in the shape of storm surge distributions. Given that the storm surge associated with each WT approximately follows a normal distribution,  $SS_{50}$  can be represented by  $\mu_{SS}$ , whereas  $SS_{99}$  is affected by both  $\mu_{SS}$  and  $\sigma_{SS}$ . Since both  $\mu_{SS}$  and  $\sigma_{SS}$  are positively correlated with NAO, a higher NAO index typically results in both a positive shift and widening of the distribution, thereby increasing  $SS_{99}$  more significantly than  $SS_{50}$ . This may also explain the lack of significant correlation with  $SS_1$ , which is positively related to  $\mu_{SS}$  but negatively to  $\sigma_{SS}$ . As such, the effects of  $\mu_{SS}$  and  $\sigma_{SS}$  counteract with each other, resulting in no significant change in  $SS_1$  in response to NAO.

The response patterns of  $\mu_{SS}$  and  $\sigma_{SS}$  are attributable to the effects of local atmospheric pressure and wind stress, both of which are modulated by large-scale climate oscillations. During NAO+/SCAND-, the synoptic circulation over Hartlepool is typically characterized by negative atmospheric pressure anomalies and enhanced westerly winds (Gleeson et al., 2019; Scott et al., 2021), which contribute to the increase in  $\mu_{SS}$  and  $\sigma_{SS}$ . In contrast, the lower  $\mu_{SS}$  and  $\sigma_{SS}$  observed during NAO-/SCAND+ are linked with positive pressure anomalies and weakened westerly winds.

## 4.3 Implications

The use of weather types to link climate oscillations with sea state variability offers several benefits. A distinctive advantage of this approach is its ability to capture response patterns through sea state distributions, offering a complementary perspective to conventional statistical analyses. For example, the modality of  $T_p$  distribution is linked with NAO and SCAND phases, a feature that cannot be captured by a simple correlation coefficient. The sensitivity of the mean and extreme storm surge to climate indices can be interpreted through the variations of  $\mu_{SS}$  and  $\sigma_{SS}$ . Moreover, the WT-based approach allows the investigation of the joint response of multiple sea state variables to climate oscillations using bi-dimensional distributions. In this work, we demonstrated the joint response pattern of wave height and wave direction through wave rose diagrams (Fig. 6). Future work could explore how climate oscillations modulate the interdependencies among other sea state parameters.

Our findings show that weather types, despite being defined over relatively short time scales (4 days in our case), can effectively link low-frequency climate variability with local sea states. This provides a strong rationale for the construction of WT-based stochastic emulators of sea state conditions (e.g., Anderson et al., 2019; Cagigal et al., 2020). These emulators are designed to generate infinitely long time series of sea state conditions for coastal risk assessments (e.g., extrapolation of extreme conditions and evaluation of long-term risk evolution). Given the role of climate variabilities in modulating coastal hazards, it is important to incorporate their influences into the emulator to construct realistic time series of sea states. In these WT-based methods, the impact of climate variabilities is introduced through some covariates (e.g., climate indices or other large-scale climatic predictors) that modulate the occurrence frequencies of WTs, which in turn produce sea state variations at the corresponding time scales. This approach enables the probabilistic assessment of the influence of climate oscillations on coastal hazards through the generation of synthetic time series (Cagigal et al., 2020).

The weather types developed in this study are tailored to the specific location using regression-guided classification to enhance downscaling performance. However, this also implies that caution should be exercised when transferring the results to other regions, particularly those with distinct geographic or oceanographic characteristics. To assess the broader applicability of our results, we calculated spatial correlations of sea state parameters across the North Sea relative to our study location (Fig.





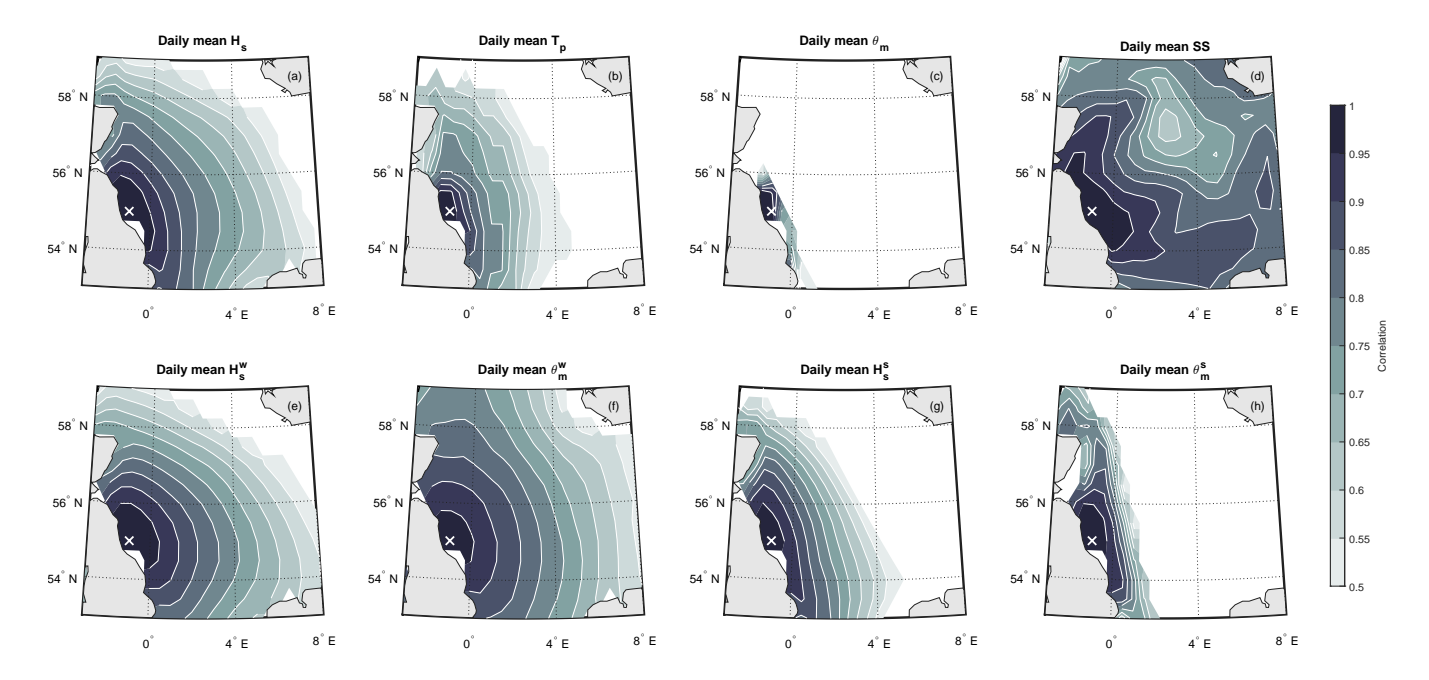


**Figure 10.** Spatial correlations of sea state parameters across the North Sea relative to our study location (indicated by a cross mark). Pearson correlation was calculated for scalar quantities, while a circular–circular correlation (Berens, 2009) was used for circular variables (i.e., wave directions). Daily mean parameters during DJFM for the period 1979–2018 were considered. Areas with no data or with correlations below 0.5 are not shown.

10). The offshore wave and storm surge conditions along the north-east coast of England exhibit very high correlations (> 0.9), which indicates similar response patterns associated with climate oscillations. This regional coherence in sea state variations was also reported in Scott et al. (2021). The correlations decrease with increasing distance from the study location, but the rate of decline varies among sea state parameters. Storm surge remains a relatively high correlation (> 0.8) across the south of the North Sea, whereas wave parameters exhibit a more rapid spatial decay. This suggests the response patterns of storm surge are transferable over a larger region than those of the wave climate.

Although the design of this research is inherently site-specific, the weather typing method itself is applicable to any location. To extend the analysis to multiple sites in a region, a single set of weather types can be developed using unsupervised classification (i.e., without tailoring to specific sites) to ensure consistency and comparability across locations. Alternatively, the weather types can be tailored to represent sea states over a larger region using the approach described by Zhao et al. (2024), which allows the investigation of the spatial variations in the impacts of climate oscillations.

## 5 Conclusions

425

430

435

In this study, we investigate the link between climate oscillations and local wave climate and storm surge conditions at Hartlepool. Our first objective is to identify the climate oscillations contributing to the local sea state variability, which was achieved



445

465



through a correlation analysis between six climate indices and wave and surge variables. Statistically significant correlations were found for NAO, SCAND, AO, and WEPA, with the first two selected for further analysis.

Our second objective focuses on characterizing the responses of wave and storm surge under the positive and negative phases of NAO/SCAND, where the WTs were introduced. Each WT and its associated sea state distributions were linked to the phases of NAO/SCAND based on the WT occurrence. The main findings are as follows: (1) the overall  $T_p$  distribution linked to NAO+/SCAND- displays bimodality, while the distribution under NAO-/SCAND+ tends toward a unimodal pattern; (2) the wave energy spectra are more frequently dominated by wind waves during NAO+/SCAND- and by swell during NAO-/SCAND+; (3) the distributions of  $\theta_m^w$  and  $\theta_m^s$  show distinct patterns regarding the dominant direction in response to climate phases; (4) the SS distributions linked to NAO+/SCAND- have higher means and standard deviations than those linked to NAO-/SCAND+.

The final objective investigates the atmospheric processes linking climate oscillations to the observed sea state responses. The fluctuations in the climate circulation patterns associated with NAO/SCAND are accompanied by changes in prevailing wind conditions, extratropical storms, and atmospheric pressure. We parametrized the impacts of these processes and related them to local sea state variability. Our analysis reveals that wind wave characteristics can be linked to local wind patterns, especially during NAO+/SCAND— when the westerly winds are strong. For swell waves, the dominant directions generally align with regions of higher storm frequency, indicating remote storm activity as a key driver. Lastly, the responses of SS distributions in terms of the mean and standard deviation show strong correlations with the inverse barometer effect and the wind forcing, respectively.

Our research demonstrates the potential of weather typing as an effective tool for linking large-scale climate dynamics to local sea state conditions. Although this study focuses on Hartlepool, the method is broadly applicable to other locations, and the findings are particularly relevant to sites along the north-east coast of England. Our results support the use of climate indices and WT-based methods in capturing sea state variability over longer time scales, which is critical to effective long-term coastal planning and risk management.

Code and data availability. The SLP and wave climate data from ERA5 reanalysis (DOI: 10.24381/cds.adbb2d47), and the storm surge data from CODEC (DOI: 10.24381/cds.a6d42d60) are publicly available at the Climate Data Store of the Copernicus Climate Change Service at https://cds.climate.copernicus.eu/. The historic indices of NAO, AO, SCAND, EA, and EA/WR are archived at the NOAA Climate Prediction Center, available at https://ftp.cpc.ncep.noaa.gov/wd52dg/data/indices/tele\_index.nh. The WEPA index Scott et al. (2020) can be obtained via the University of Plymouth PEARL open access research repository. The processed data and MATLAB codes used in this research are available at Zenodo under a Creative Commons Attribution 4.0 International Public License.

## Appendix A: Additional figures





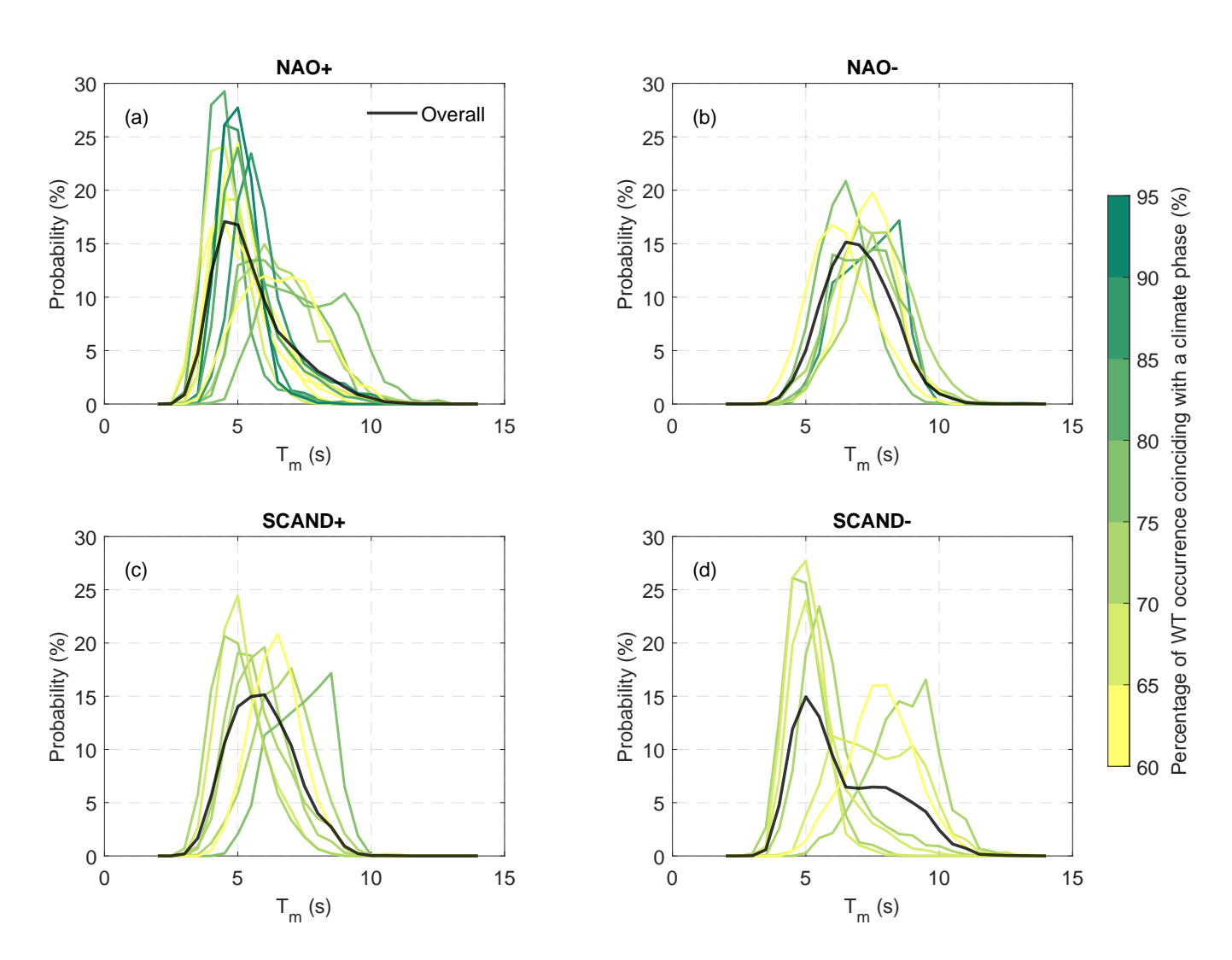


Figure A1. The empirical distributions of hourly  $T_m$  associated with NAO and SCAND phases (similar to Fig. 4).





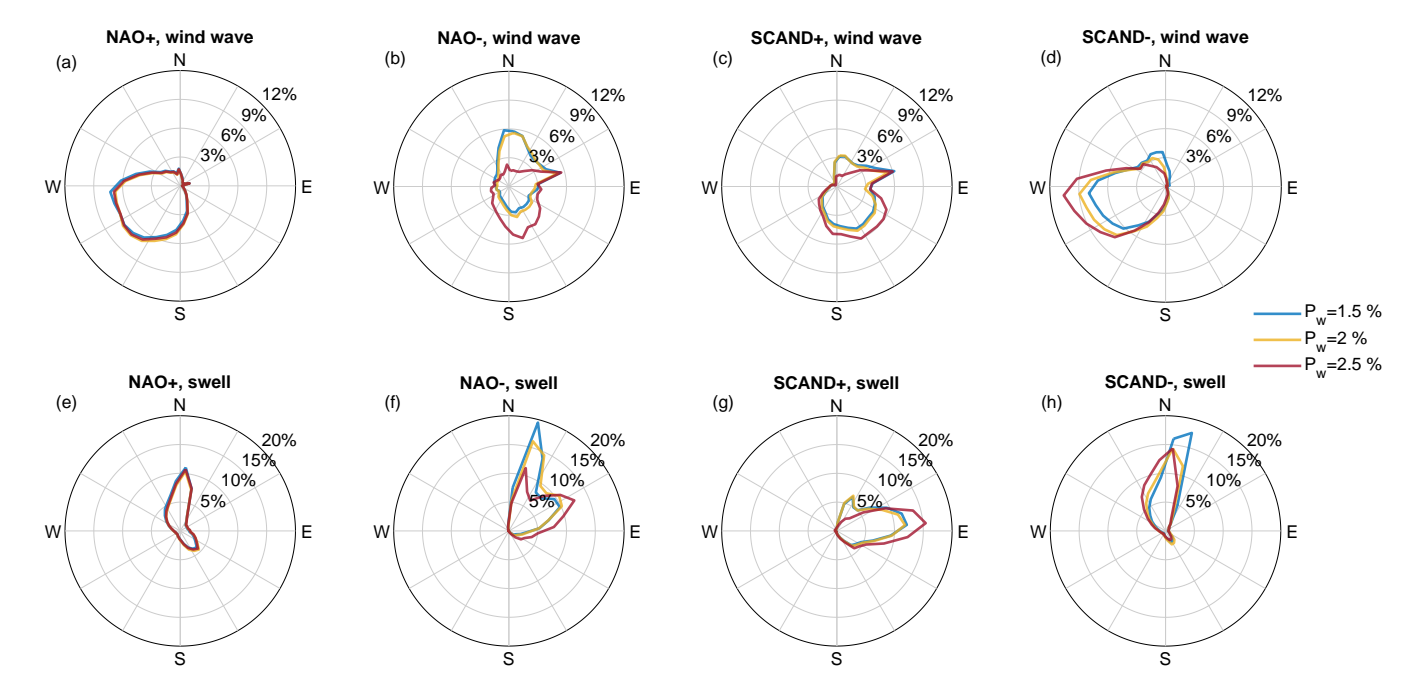


Figure A2. Sensitivity analysis of the impact of  $P_w$  in WT categorization on wave direction distributions





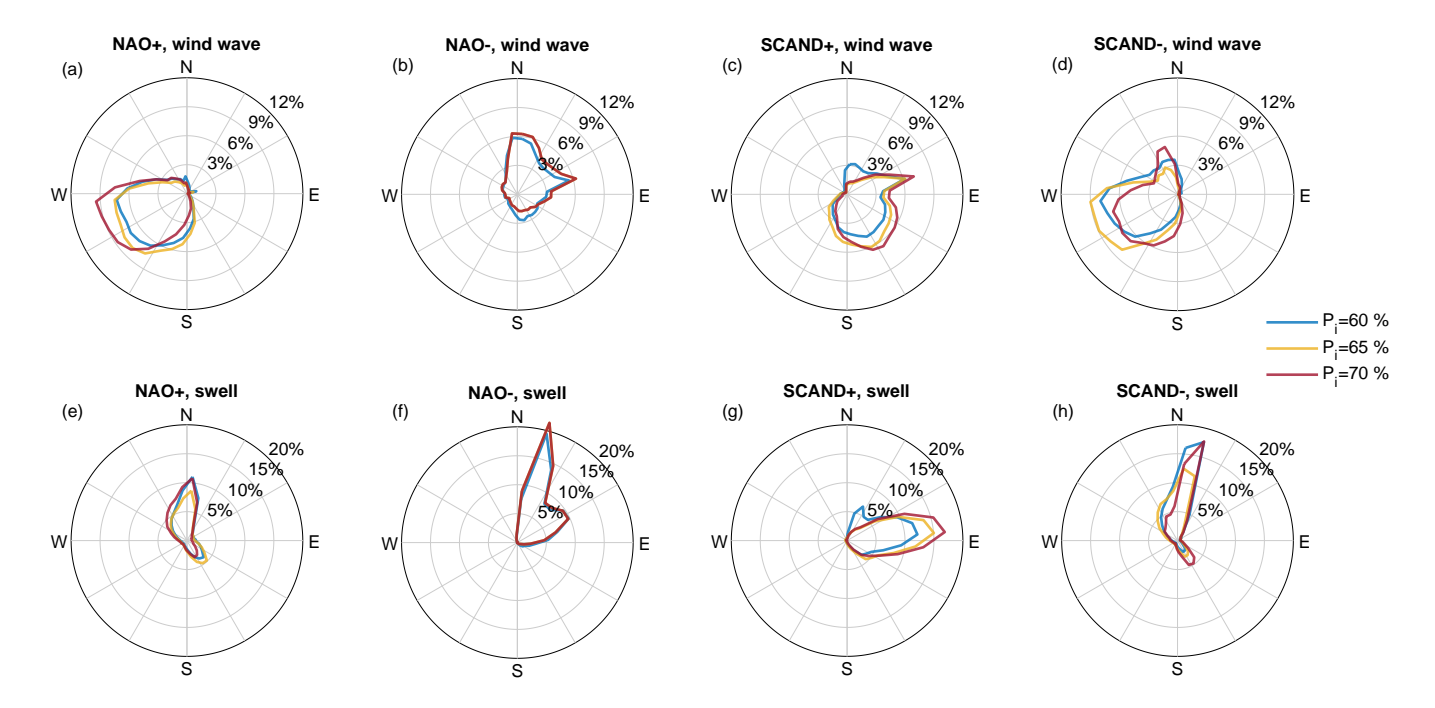
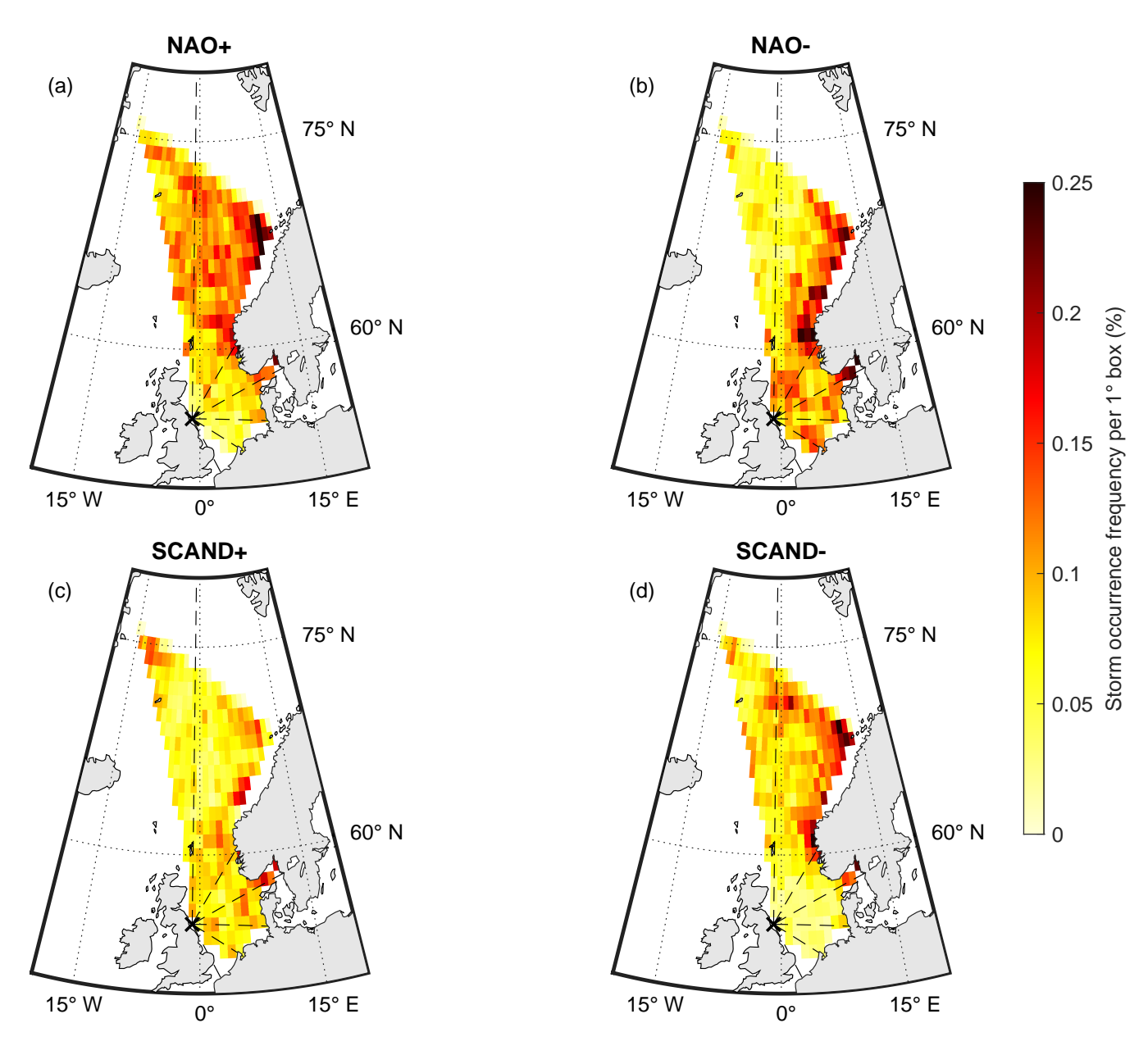


Figure A3. Sensitivity analysis of the impact of  $P_i$  in WT categorization on wave direction distributions







**Figure A4.** Spatial distribution of storm occurrence frequency associated with NAO and SCAND phases, similar to Fig. 9. The association of storms with climate phases is based on monthly climate indices.





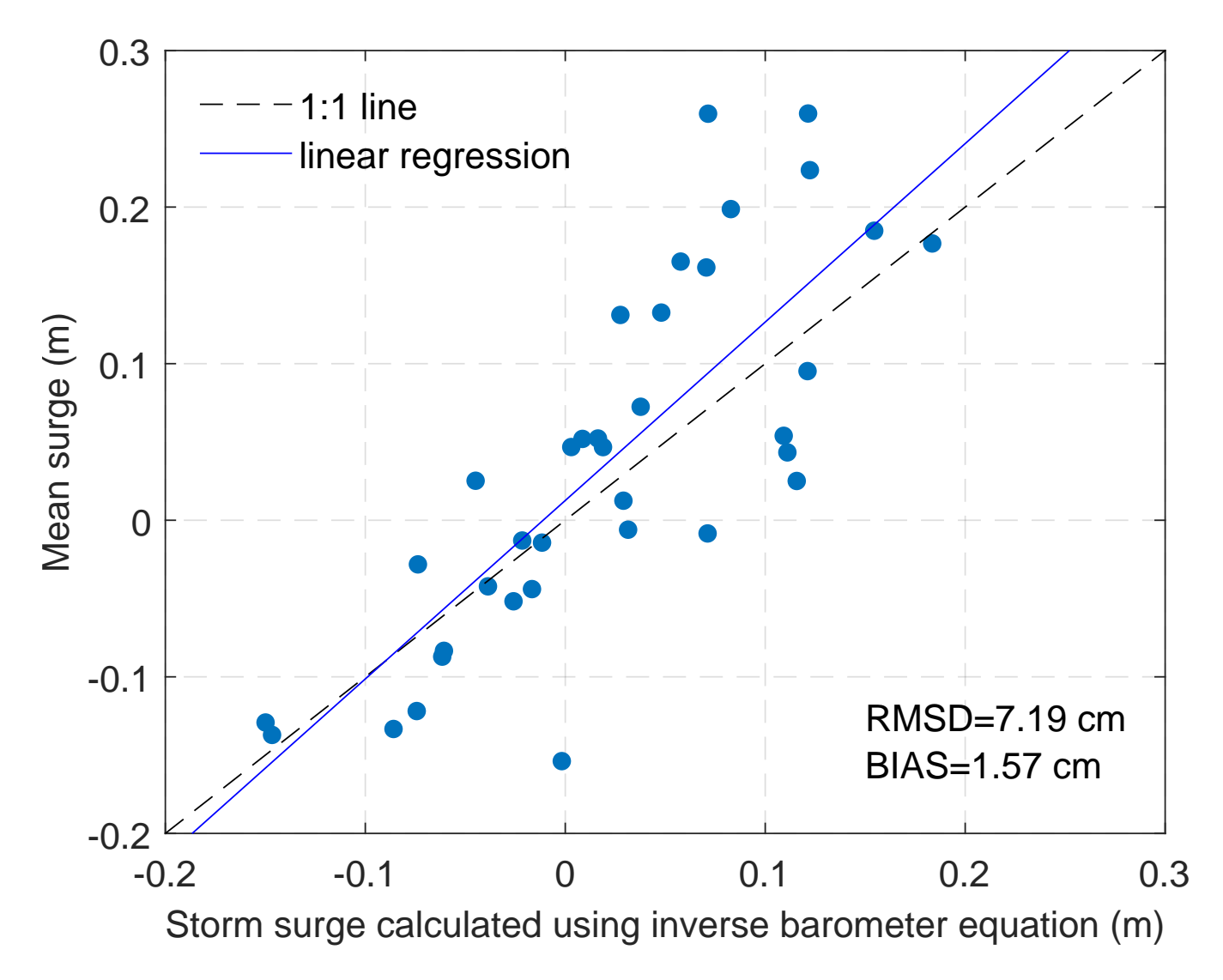


**Figure A5.** Comparison between estimated storm surges caused by inverse barometer effect and the mean of storm surge distribution associated with each WT.





Appendix B: Additional tables





Table B1. WT categorization based on the percentage of occurrence coinciding a positive or negative index during DJFM.

	-					-
WT	Probability during DJFM	NAO>0	NAO<0	SCAND>0	SCAND<0	Category
1	2.40 %	88.79 %	11.21 %	25.00 %	71.55 %	NAO+, SCAND-
2	2.37 %	50.43 %	49.57 %	70.43 %	28.70 %	SCAND+
3	6.07 %	63.95 %	33.67 %	49.32 %	48.64 %	NAO+
4	2.70 %	45.04 %	54.96 %	71.76 %	26.72 %	SCAND+
5	3.12 %	41.06 %	58.94 %	72.85 %	27.15 %	SCAND+
6	1.94 %	13.83 %	86.17 %	79.79 %	20.21 %	NAO-, SCAND+
7	3.16 %	62.09 %	36.60 %	67.97 %	31.37 %	NAO+, SCAND+
8	5.43 %	66.92 %	33.08 %	47.53 %	51.71 %	NAO+
9	2.68 %	46.92 %	50.77 %	70.00 %	30.00 %	SCAND+
10	3.96 %	47.92 %	52.08 %	40.63 %	57.29 %	-
11	0.76 %	51.35 %	48.65 %	72.97 %	27.03 %	-
12	2.44 %	22.88 %	77.12 %	62.71 %	37.29 %	NAO-, SCAND+
13	4.65 %	81.78 %	16.00 %	46.67 %	53.33 %	NAO+
14	3.28 %	69.81 %	28.30 %	49.06 %	50.31 %	NAO+
15	1.59 %	62.34 %	37.66 %	50.65 %	49.35 %	NAO+
16	0.66 %	71.88 %	28.13 %	46.88 %	53.13 %	-
17	1.01 %	63.27 %	36.73 %	44.90 %	55.10 %	-
18	3.94 %	35.60 %	64.40 %	59.69 %	40.31 %	NAO-
19	4.25 %	70.87 %	24.27 %	41.26 %	58.25 %	NAO+
20	3.20 %	76.13 %	23.87 %	40.00 %	60.00 %	NAO+
21	1.05 %	76.47 %	23.53 %	31.37 %	68.63 %	-
22	0.19 %	33.33 %	66.67 %	77.78 %	11.11 %	-
23	1.61 %	42.31 %	56.41 %	47.44 %	52.56 %	-
24	4.40 %	28.17 %	71.83 %	50.23 %	49.77 %	NAO-
25	2.73 %	87.88 %	12.12 %	24.24 %	74.24 %	NAO+, SCAND-
26	2.60 %	78.57 %	21.43 %	34.13 %	65.87 %	NAO+, SCAND-
27	2.15 %	52.88 %	47.12 %	27.88 %	72.12 %	SCAND-
28	0.54 %	57.69 %	42.31 %	76.92 %	23.08 %	-
29	2.11 %	38.24 %	61.76 %	55.88 %	44.12 %	NAO-
30	2.70 %	24.43 %	75.57 %	48.85 %	51.15 %	NAO-
31	3.18 %	90.91 %	9.09 %	32.47 %	66.23 %	NAO+, SCAND-
32	5.60 %	82.29 %	17.71 %	31.37 %	67.53 %	NAO+, SCAND-
33	3.88 %	62.23 %	37.77 %	43.09 %	56.38 %	NAO+
34	3.16 %	46.41 %	53.59 %	45.75 %	54.25 %	-
35	2.68 %	52.31 %	47.69 %	47.69 %	52.31 %	-
36	1.80 %	29.89 %	70.11 %	37.93 %	62.07 %	NAO-, SCAND-





**Table B2.** Distributions and statistics of  $H_s^w$  and  $H_s^s$  associated with NAO and SCAND phases. P(X) denotes the occurrence probability of X.

	NAO+	NAO-	SCAND+	SCAND-
Mean $H_s^w$	0.86 m	0.82 m	0.79 m	1.16 m
$P(H_s^w < 1)$	65.5 %	70.1 %	70.9 %	46.8 %
$P(1 \le H_s^w \le 2)$	29.0 %	21.7 %	22.9 %	40.4 %
$P(H_s^w > 2)$	5.4 %	8.2 %	6.2 %	12.7 %
$P(H_s^w > H_s^s)$	55.8 %	20.5 %	30.8 %	55.7 %
Mean $H_s^s$	0.72 m	1.33 m	1.03 m	1.05 m
$P(H_s^s < 1)$	80.5 %	30.0 %	55.2 %	58.4 %
$P(1 \le H_s^s \le 2)$	17.4 %	58.0 %	38.9 %	31.4 %
$P(H_s^s > 2)$	2.0 %	12.0 %	5.9 %	10.2 %
$P(H_s^w < H_s^s)$	44.2 %	79.5 %	69.2 %	44.3 %





**Table B3.** Sensitivity analysis of the method for associating WTs with climate oscillations. The influence of the two threshold values on storm surge and wave climate characteristics linked to NAO and SCAND phases was evaluated. In the baseline case,  $P_w$  and  $P_i$  are set to 1.5 % and 60 %, respectively (i.e., the values used in Table B1).

		Baseline	$P_w$ =2 %	<i>P</i> <sub>w</sub> =2.5 %	P <sub>i</sub> =65 %	P <sub>i</sub> =75 %
$\mu_{SS}$ (m)	NAO+	0.09	0.10	0.10	0.14	0.18
	NAO-	-0.01	0.00	0.04	-0.01	-0.01
	SCAND+	-0.05	-0.04	-0.06	-0.05	-0.10
	SCAND-	0.16	0.20	0.21	0.20	0.21
$\sigma_{SS}$ (m)	NAO+	0.25	0.26	0.25	0.25	0.27
	NAO-	0.17	0.17	0.18	0.16	0.16
	SCAND+	0.19	0.20	0.20	0.21	0.19
	SCAND-	0.28	0.29	0.29	0.29	0.30
Mean $H_s^w$ (m)	NAO+	0.86	0.90	0.88	0.97	1.11
	NAO-	0.82	0.79	0.75	0.79	0.79
	SCAND+	0.79	0.74	0.72	0.82	0.88
	SCAND-	1.16	1.26	1.22	1.26	1.38
Mean $H_s^s$ (m)	NAO+	0.72	0.74	0.74	0.73	0.81
	NAO-	1.33	1.27	1.22	1.35	1.35
	SCAND+	1.03	0.98	0.91	0.98	1.18
	SCAND-	1.05	0.97	0.84	0.97	1.17
$P(H_s^w > H_s^s)(\%)$	NAO+	55.8	57.3	56.2	62.9	66.0
	NAO-	20.5	21.3	23.7	17.4	17.4
	SCAND+	30.8	30.9	33.4	35.6	27.6
	SCAND-	55.7	65.3	68.8	65.3	62.2
$P(H_s^w < H_s^s)(\%)$	NAO+	44.2	42.7	43.8	37.0	34.0
	NAO-	79.5	78.7	76.3	82.6	82.6
	SCAND+	69.2	69.1	66.6	64.4	72.4
	SCAND-	44.3	34.7	31.2	34.7	37.8





Author contributions. Z.Z.: Conceptualization, Data curation, Formal analysis, Investigation, Software, Validation, Visualization, Writing—review & editing. H.K.: Conceptualization, Funding acquisition, Supervision, Writing—review & editing. I.D.H.: Supervision, Writing—review & editing. D.E.S.: Funding acquisition, Supervision, Writing—review & editing. Y.L.: Supervision, Writing—review & editing. P.C.: Methodology, Software, Writing—review & editing.

Competing interests. The authors declare that they have no conflict of interest.

*Acknowledgements*. This project is funded through the INSPIRE Doctoral Training Partnership by the Natural Environment Research Council (NERC) (NE/S007210/1; project reference: 2740403), and co-sponsored by EDF Energy.





#### References

- Ambaum, M. H. P., Hoskins, B. J., and Stephenson, D. B.: Arctic Oscillation or North Atlantic Oscillation?, Journal of Climate, 14, 3495–3507, https://doi.org/10.1175/1520-0442(2001)014<3495:AOONAO>2.0.CO;2, 2001.
  - Anderson, D., Rueda, A., Cagigal, L., Antolinez, J. A. A., Mendez, F. J., and Ruggiero, P.: Time-Varying Emulator for Short and Long-Term Analysis of Coastal Flood Hazard Potential, Journal of Geophysical Research: Oceans, 124, 9209–9234, https://doi.org/10.1029/2019JC015312, 2019.
- 480 Arcodia, M. C., Becker, E., and Kirtman, B. P.: Subseasonal Variability of U.S. Coastal Sea Level from MJO and ENSO Teleconnection Interference, Weather and Forecasting, https://doi.org/10.1175/WAF-D-23-0002.1, 2024.
  - Barnard, P. L., Short, A. D., Harley, M. D., Splinter, K. D., Vitousek, S., Turner, I. L., Allan, J., Banno, M., Bryan, K. R., Doria, A., Hansen, J. E., Kato, S., Kuriyama, Y., Randall-Goodwin, E., Ruggiero, P., Walker, I. J., and Heathfield, D. K.: Coastal vulnerability across the Pacific dominated by El Niño/Southern Oscillation, Nature Geoscience, 8, 801–807, https://doi.org/10.1038/ngeo2539, 2015.
- Barnston, A. G. and Livezey, R. E.: Classification, Seasonality and Persistence of Low-Frequency Atmospheric Circulation Patterns, Monthly Weather Review, 115, 1083–1126, https://doi.org/10.1175/1520-0493(1987)115<1083:CSAPOL>2.0.CO;2, 1987.
  - Berens, P.: CircStat: A MATLAB Toolbox for Circular Statistics, Journal of Statistical Software, 31, 1–21, https://doi.org/10.18637/jss.v031.i10, 2009.
- Cagigal, L., Rueda, A., Anderson, D., Ruggiero, P., Merrifield, M. A., Montaño, J., Coco, G., and Méndez, F. J.:

  490 A multivariate, stochastic, climate-based wave emulator for shoreline change modelling, Ocean Modelling, 154, 101695, https://doi.org/10.1016/j.ocemod.2020.101695, 2020.
  - Camus, P., Menéndez, M., Méndez, F. J., Izaguirre, C., Espejo, A., Cánovas, V., Pérez, J., Rueda, A., Losada, I. J., and Medina, R.: A weather-type statistical downscaling framework for ocean wave climate, Journal of Geophysical Research: Oceans, 119, 7389–7405, https://doi.org/10.1002/2014JC010141, 2014.
- 495 Camus, P., Rueda, A., Méndez, F. J., and Losada, I. J.: An atmospheric-to-marine synoptic classification for statistical downscaling marine climate, Ocean Dynamics, 66, 1589–1601, https://doi.org/10.1007/s10236-016-1004-5, 2016.
  - Camus, P., Haigh, I. D., Quinn, N., Wahl, T., Benson, T., Gouldby, B., Nasr, A. A., Rashid, M. M., Enríquez, A. R., Darby, S. E., Nicholls, R. J., and Nadal-Caraballo, N. C.: Tracking the spatial footprints of extreme storm surges around the coastline of the UK and Ireland, Weather and Climate Extremes, 44, 100 662, https://doi.org/10.1016/j.wace.2024.100662, 2024.
- Casas-Prat, M., Hemer, M. A., Dodet, G., Morim, J., Wang, X. L., Mori, N., Young, I., Erikson, L., Kamranzad, B., Kumar, P., Menéndez, M., and Feng, Y.: Wind-wave climate changes and their impacts, Nature Reviews Earth & Environment, 5, 23–42, https://doi.org/10.1038/s43017-023-00502-0, 2024.
  - Cassou, C., Terray, L., Hurrell, J. W., and Deser, C.: North Atlantic Winter Climate Regimes: Spatial Asymmetry, Stationarity with Time, and Oceanic Forcing, Journal of Climate, 17, 1055–1068, https://doi.org/10.1175/1520-0442(2004)017<1055:NAWCRS>2.0.CO;2, 2004.
- Castelle, B., Dodet, G., Masselink, G., and Scott, T.: A new climate index controlling winter wave activity along the Atlantic coast of Europe: The West Europe Pressure Anomaly, Geophysical Research Letters, 44, 1384–1392, https://doi.org/https://doi.org/10.1002/2016GL072379, 2017.
  - Castelle, B., Dodet, G., Masselink, G., and Scott, T.: Increased Winter-Mean Wave Height, Variability, and Periodicity in the Northeast Atlantic Over 1949-2017, Geophysical Research Letters, 45, 3586–3596, https://doi.org/https://doi.org/10.1002/2017GL076884, 2018.



525

530

540



- 510 Chafik, L., Nilsen, J. E. ø., and Dangendorf, S.: Impact of North Atlantic Teleconnection Patterns on Northern European Sea Level, Journal of Marine Science and Engineering, 5, 43, https://doi.org/10.3390/jmse5030043, 2017.
  - Frederikse, T. and Gerkema, T.: Multi-decadal variability in seasonal mean sea level along the North Sea coast, Ocean Science, 14, 1491–1501, https://doi.org/10.5194/os-14-1491-2018, 2018.
- Freitas, A., Bernardino, M., and Guedes Soares, C.: The influence of the Arctic Oscillation on North Atlantic wind and wave climate by the end of the 21st century, Ocean Engineering, 246, 110 634, https://doi.org/10.1016/j.oceaneng.2022.110634, 2022.
  - Gleeson, E., Clancy, C., Zubiate, L., Janjić, J., Gallagher, S., and Dias, F.: Teleconnections and Extreme Ocean States in the Northeast Atlantic Ocean, in: Advances in Science and Research, vol. 16, pp. 11–29, Copernicus GmbH, https://doi.org/10.5194/asr-16-11-2019, 2019.
- Gulev, S. K. and Grigorieva, V.: Variability of the Winter Wind Waves and Swell in the North Atlantic and North Pacific as Revealed by the Voluntary Observing Ship Data, Journal of Climate, 19, 5667–5685, https://doi.org/10.1175/JCLI3936.1, 2006.
  - Gulev, S. K., Zolina, O., and Grigoriev, S.: Extratropical cyclone variability in the Northern Hemisphere winter from the NCEP/NCAR reanalysis data, Climate Dynamics, 17, 795–809, https://doi.org/10.1007/s003820000145, 2001.
  - Haigh, I. D., Wadey, M. P., Wahl, T., Ozsoy, O., Nicholls, R. J., Brown, J. M., Horsburgh, K., and Gouldby, B.: Spatial and temporal analysis of extreme sea level and storm surge events around the coastline of the UK, Scientific Data, 3, 160107, https://doi.org/10.1038/sdata.2016.107, 2016.
  - Hersbach, H., Bell, B., Berrisford, P., Hirahara, S., Horányi, A., Muñoz Sabater, J., Nicolas, J., Peubey, C., Radu, R., Schepers, D., Simmons, A., Soci, C., Abdalla, S., Abellan, X., Balsamo, G., Bechtold, P., Biavati, G., Bidlot, J., Bonavita, M., De Chiara, G., Dahlgren, P., Dee, D., Diamantakis, M., Dragani, R., Flemming, J., Forbes, R., Fuentes, M., Geer, A., Haimberger, L., Healy, S., Hogan, R. J., Hólm, E., Janisková, M., Keeley, S., Laloyaux, P., Lopez, P., Lupu, C., Radnoti, G., de Rosnay, P., Rozum, I., Vamborg, F., Villaume, S., and Thépaut, J.-N.: The ERA5 global reanalysis, Quarterly Journal of the Royal Meteorological Society, 146, 1999–2049, https://doi.org/10.1002/qj.3803, 2020.
  - Hilton, D., Davidson, M., and Scott, T.: Seasonal Predictions of Shoreline Change, Informed by Climate Indices, Journal of Marine Science and Engineering, 8, 616, https://doi.org/10.3390/jmse8080616, 2020.
- Hochet, A., Dodet, G., Ardhuin, F., Hemer, M., and Young, I.: Sea State Decadal Variability in the North Atlantic: A Review, Climate, 9, 173, https://doi.org/10.3390/cli9120173, 2021.
  - Hurrell, J. W.: Decadal Trends in the North Atlantic Oscillation: Regional Temperatures and Precipitation, Science, 269, 676–679, https://doi.org/10.1126/science.269.5224.676, 1995.
  - Hurrell, J. W., Kushnir, Y., Ottersen, G., and Visbeck, M.: An Overview of the North Atlantic Oscillation: Climatic Significance and Environmental Impact, pp. 1–35, American Geophysical Union (AGU), ISBN 978-1-118-66903-7, https://doi.org/10.1029/134GM01, 2003.
  - Itoh, H.: Reconsideration of the True versus Apparent Arctic Oscillation, Journal of Climate, 21, 2047–2062, https://doi.org/10.1175/2007JCLI2167.1, 2008.
  - Lamb, P. J. and Peppler, R. A.: North Atlantic Oscillation: Concept and an Application, Bulletin of the American Meteorological Society, 1987
- Martínez-Asensio, A., Tsimplis, M. N., Marcos, M., Feng, X., Gomis, D., Jordà, G., and Josey, S. A.: Response of the North Atlantic wave climate to atmospheric modes of variability, International Journal of Climatology, 36, 1210–1225, https://doi.org/10.1002/joc.4415, 2016.



550

565



- Masselink, G., Castelle, B., Scott, T., and Konstantinou, A.: Role of Atmospheric Indices in Describing Shoreline Variability Along the Atlantic Coast of Europe, Geophysical Research Letters, 50, e2023GL106019, https://doi.org/10.1029/2023GL106019, 2023.
- Michelangeli, P.-A., Vautard, R., and Legras, B.: Weather Regimes: Recurrence and Quasi Stationarity, Journal of Atmospheric Sciences, 52, 123–1256, https://doi.org/10.1175/1520-0469(1995)052<1237:WRRAOS>2.0.CO;2, 1995.
  - Morales-Márquez, V., Orfila, A., Simarro, G., and Marcos, M.: Extreme waves and climatic patterns of variability in the eastern North Atlantic and Mediterranean basins, Ocean Science, 16, 1385–1398, https://doi.org/10.5194/os-16-1385-2020, 2020.
  - Muis, S., Haigh, I. D., Guimarães Nobre, G., Aerts, J. C. J. H., and Ward, P. J.: Influence of El Niño-Southern Oscillation on Global Coastal Flooding, Earth's Future, 6, 1311–1322, https://doi.org/10.1029/2018EF000909, 2018.
- Muis, S., Apecechea, M. I., Dullaart, J., de Lima Rego, J., Madsen, K. S., Su, J., Yan, K., and Verlaan, M.: A High-Resolution Global Dataset of Extreme Sea Levels, Tides, and Storm Surges, Including Future Projections, Frontiers in Marine Science, 7, https://doi.org/10.3389/fmars.2020.00263, 2020.
  - Neal, R., Fereday, D., Crocker, R., and Comer, R. E.: A flexible approach to defining weather patterns and their application in weather forecasting over Europe, Meteorological Applications, 23, 389–400, https://doi.org/10.1002/met.1563, 2016.
- Odériz, I., Silva, R., Mortlock, T. R., and Mori, N.: El Niño-Southern Oscillation Impacts on Global Wave Climate and Potential Coastal Hazards, Journal of Geophysical Research: Oceans, 125, https://doi.org/10.1029/2020JC016464, 2020.
  - Pohl, B. and Fauchereau, N.: The Southern Annular Mode Seen through Weather Regimes, Journal of Climate, 25, 3336–3354, https://doi.org/10.1175/JCLI-D-11-00160.1, 2012.
  - Pugh, D. and Woodworth, P.: Storm surges, meteotsunamis and other meteorological effects on sea level, pp. 155–188, Cambridge University Press, 2014.
    - Pérez, J., Méndez, F. J., Menéndez, M., and Losada, I. J.: ESTELA: a method for evaluating the source and travel time of the wave energy reaching a local area, Ocean Dynamics, 64, 1181–1191, https://doi.org/10.1007/s10236-014-0740-7, 2014.
    - Scott, T., Masselink, G., Castelle, B., and Dodet, G.: The West Europe Pressure Anomaly: 1943–2018, https://doi.org/10.24382/35ae12b5-df54-479d-ad09-75ea5049d14f, 2020.
- 570 Scott, T., McCarroll, R. J., Masselink, G., Castelle, B., Dodet, G., Saulter, A., Scaife, A. A., and Dunstone, N.: Role of Atmospheric Indices in Describing Inshore Directional Wave Climate in the United Kingdom and Ireland, Earth's Future, 9, e2020EF001625, https://doi.org/10.1029/2020EF001625, 2021.
  - Semedo, A., Sušelj, K., Rutgersson, A., and Sterl, A.: A Global View on the Wind Sea and Swell Climate and Variability from ERA-40, Journal of Climate, https://doi.org/10.1175/2010JCLI3718.1, 2011.
- 575 Semedo, A., Vettor, R., Breivik, O., Sterl, A., Reistad, M., Soares, C. G., and Lima, D.: The wind sea and swell waves climate in the Nordic seas, Ocean Dynamics, 65, 223–240, https://doi.org/10.1007/s10236-014-0788-4, 2015.
  - Shimura, T., Mori, N., and Mase, H.: Ocean Waves and Teleconnection Patterns in the Northern Hemisphere, Journal of Climate, 26, 8654–8670, https://doi.org/10.1175/JCLI-D-12-00397.1, 2013.
- Wakelin, S. L., Woodworth, P. L., Flather, R. A., and Williams, J. A.: Sea-level dependence on the NAO over the NW European Continental Shelf, Geophysical Research Letters, 30, https://doi.org/10.1029/2003GL017041, 2003.
  - Wang, X. L. and Swail, V. R.: Changes of Extreme Wave Heights in Northern Hemisphere Oceans and Related Atmospheric Circulation Regimes, Journal of Climate, 14, 2204–2221, https://doi.org/10.1175/1520-0442(2001)014<2204:COEWHI>2.0.CO;2, 2001.
  - Wiggins, M., Scott, T., Masselink, G., McCarroll, R. J., and Russell, P.: Predicting beach rotation using multiple atmospheric indices, Marine Geology, 426, 106 207, https://doi.org/10.1016/j.margeo.2020.106207, 2020.



590



- Wilby, R. and Wigley, T.: Downscaling general circulation model output: a review of methods and limitations, Progress in Physical Geography: Earth and Environment, 21, 530–548, https://doi.org/10.1177/030913339702100403, 1997.
  - Woodworth, P. L., Flather, R. A., Williams, J. A., Wakelin, S. L., and Jevrejeva, S.: The dependence of UK extreme sea levels and storm surges on the North Atlantic Oscillation, Continental Shelf Research, 27, 935–946, https://doi.org/10.1016/j.csr.2006.12.007, 2007.
  - Woolf, D. K., Challenor, P. G., and Cotton, P. D.: Variability and predictability of the North Atlantic wave climate, Journal of Geophysical Research: Oceans, 107, 9–1–9–14, https://doi.org/10.1029/2001JC001124, 2002.
  - Zhao, G., Li, D., Yang, S., Qi, J., and Yin, B.: The development of a weather-type statistical downscaling model for wave climate based on wave clustering, Ocean Engineering, 304, 117 863, https://doi.org/10.1016/j.oceaneng.2024.117863, 2024.
  - Zhong, Z., Kassem, H., Haigh, I. D., Sifnioti, D. E., Gouldby, B., Liu, Y., and Camus, P.: Advanced weather typing for downscaling of wave climate and storm surge at a UK nuclear power station, Ocean Dynamics, 75, 32, https://doi.org/10.1007/s10236-025-01682-7, 2025.